RESEARCH ARTICLE

Basin Research · IAS EAGE · WILEY

Heat flow and thermal regime in the Guaymas Basin, Gulf of California: Estimates of conductive and advective heat transport

Florian Neumann[1] | Raquel Negrete-Aranda[1] | Robert N. Harris[2] | Juan Contreras[1] | Christophe Y. Galerne[3] | Manet S. Peña-Salinas[4] | Ronald M. Spelz[4] | Andreas Teske[5] | Daniel Lizarralde[6] | Tobias W. Höfig[7] | Expedition 385 Scientists

[1]Tectonophysics and Heat Flow Laboratory, CICESE, Centro de Investigación Científica y de Educación Superior de Ensenada, Ensenada, Mexico

[2]CEOAS, College of Earth, Ocean, and Atmospheric Sciences, Oregon State University, Corvallis, Oregon, USA

[3]Department of Geosciences, Section Petrology of the Ocean Crust, University of Bremen, Bremen, Germany

[4]Departamento de Geología, Facultad de Ciencias Marinas, Universidad Autónoma de Baja California, Ensenada, Mexico

[5]Department of Earth, Marine and Environmental Sciences, University of North Carolina at Chapel Hill, North Carolina, Chapel Hill, USA

[6]Department of Geology and Geophysics, Woods Hole Oceanographic Institution, Woods Hole, Massachusetts, USA

[7]International Ocean Discovery Program, Texas A&M University, College Station, Texas, USA

Correspondence
Florian Neumann, GFZ, German Research Centre for Geosciences, Section 4.8 Geoenergy, Telegrafenberg, 14473 Potsdam, Germany.
Email: florian.neumann@gfz-potsdam.de

Abstract

Heat flow is estimated at eight sites drilled int the Guaymas Basin, Gulf of California, during the International Ocean Discovery Program Expedition 385. The expedition sought to understand the thermal regime of the basin and heat transfer between off-axis sills intruding the organic-rich sediments of the Guaymas Basin, and the basin floor. The distinct sedimentation rates, active tectonics, and magmatism make the basin interesting for scientific discoveries. Results show that sedimentation corrected heat flow values range 119–221 mW/m^2 in the basin and 257–1003 mW/m^2 at the site of a young sill intrusion, denominated Ringvent. Thermal analysis shows that heat in the Guaymas Basin is being dissipated by conduction for plate ages >0.2 Ma, whereas younger plate ages are in a state of transient cooling by both conduction and advection. Drilling sites show that Ringvent is an active sill being cooled down slowly by circulating fluids with discharge velocities of 10–200 mm/yr. Possible recharge sites are located ca. 1 km away from the sill's border. Modelling of the heat output at Ringvent indicates a sill thickness of ca. 240 m. A simple order-of-magnitude model predicts that relatively small amounts of magma are needed to account for the elevated heat flow in non-volcanic, sediment-filled rifts like the central and northern Gulf of California in which heating of the upper crust is achieved via advection by sill emplacement and hydrothermal circulation. Multiple timescales of cooling control the crustal, chemical and biological evolution of the Guaymas Basin. Here, we recognize at least four timescales: the time interval between intrusions (ca. 10^3 yr), the thermal relaxation time of sills (ca. 10^4 yr), the characteristic cooling time of the sediments (ca. 10^5 yr), and the cooling of the entire crust at geologic timescales.

Present address
Florian Neumann, GFZ, German
Research Center for Geosciences,
Section 4.8 Geoenergy, Telegrafenberg,
14473, Potsdam, Germany

Tobias W. Höfig, Project Management
Jülich, Coastal, Marine, and Polar
Research, Research Centre Jülich (FZJ),
18069, Rostock, Germany

1 | INTRODUCTION

The Expedition 385 *Guaymas Basin Tectonics and Biosphere* of the International Ocean Discovery Program (IODP) has been designed to advance our understanding of the physical, chemical, and biological processes associated with magmatic sills intruded into organic-rich sediment (Einsele et al., 1980; Saunders et al., 1982; Teske et al., 2021a). Heat released from these intrusions is an important agent in producing and liberating CO_2, CH_4, and petroleum from organic-rich sediment (e.g., Svensen et al., 2004). The heat liberated also drives hydrothermal fluid circulation through the sill/sediment sequences that can transport these products to the seafloor, the water column, and possibly the atmosphere, where they contribute to the greenhouse effect (Aarnes et al., 2010; Berndt et al., 2016; Galerne & Hasenclever, 2019; Iyer et al., 2013; Kawka & Simoneit, 1987; Simoneit & Kawka, 1987; Von Damm et al., 1985). Additionally, because microbial ecology is energy-dependent, temperature measurements were particularly useful during Expedition 385 to help formulate a microbiological sampling strategy.

The thermal regime of rift zones like the Guaymas Basin (GB) in the Gulf of California (GOC) is controlled by the supply of heat at the base of the lithosphere, the decay of radioactive isotopes, chemical reactions, phase transitions, and heat loss at the surface (Figure 1). This regime, in turn, is modified by spatial and temporal variations in sedimentation as well as by changes in thermal and other petrophysical properties like permeability that modulate the heat transferred through the lithosphere by conduction and advection. Heat, ultimately, controls and facilitates rifting (e.g., Leroy et al., 2010; Lizarralde et al., 2007).

Highlights

- Estimation of heat flow in the Guaymas Basin from deep ocean boreholes.
- Thermal processes of igneous sill intrusions into organic-rich sediment.
- Discuss the extend of hydrothermal circulation, and the conductive heat flow throughout the basin.
- We show that small amounts of magma are required to keep rifting going.

To get more details about how these processes interact with each other, six sites were drilled in the northwestern part of the basin, one at the ridge axis in the northern trough close to Deep Sea Drilling Project (DSDP) Leg 64 Site 481 and one on the eastern side of the basin (Figure 1a). Two sites were drilled within or in the vicinity of Ringvent, a ring-shaped structure, characterized by significant thermal anomalies (Teske et al., 2019, Figure 1b). Only three sites are in areas of previously collected shallow heat flow measurements (e.g., Fisher & Becker, 1991; Geilert et al., 2018; Williams et al., 1979) and five sites cover areas with no previously estimated heat flow values. In this study, we report and analyse formation temperature and thermal conductivity measurements obtained during the IODP Expedition 385. These measurements allow us to accurately constrain the temperature and thermal properties of sediment cores from which we obtain precise estimates of heat flow, heat budget, heat transfer mechanisms, and the thermal impact on the sediment during the thermal evolution of these sill intrusions. Our results, in combination with previous
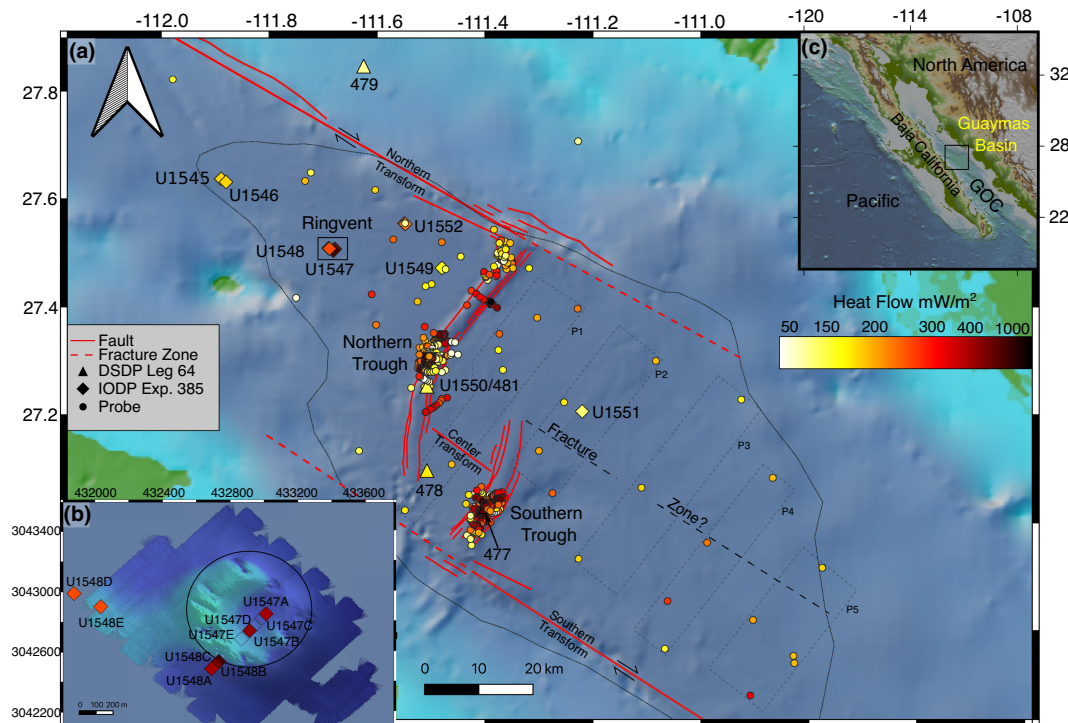
FIGURE 1 Tectonic setting of the Guaymas Basin. (a) Shallow heat flow measurements (circles) and drilled sites during DSDP/IODP Expedition 64 (triangles) and 385 (squares), respectively. Faults (red solid lines) are taken from Lonsdale (1989). Rectangles represent heat flow profiles shown in Figure 6b. (b) Sites drilled at the Ringvent structure during IODP Expedition 385 (modified from Teske et al., 2019). Open squares represent holes, without temperature measurement and therefore no heat flow estimate was obtained (Table 1). (c) Overview map with location of the Guaymas Basin within the Gulf of California.

heat flow surveys, illustrate the complicated thermal setting apparent in the Guaymas Basin. These observations provide evidence on advective cooling of a recent sill intrusion in a highly sedimented young rift setting. We attempt to separate from the total heat flow, the conductive and advective components and their timescales to extract relationships between tectonic setting, basin thermal regime, and hydrothermal activity.

2 | GUAYMAS BASIN

The GB is the largest of the enclosed basins in the GOC with a width of ~100 km (Figure 1a). It is a young seafloor spreading centre where new oceanic crust is being formed in an environment of rapid sedimentation (Calvert, 1966; Lizarralde et al., 2007). The basin floor reaches a maximum depth of ~2.1 km bsl and contains two large northeast-trending grabens: the northern and southern troughs. They are 40 and 20 km long, respectively, and 3–4 km wide each (Figure 1a). These structures are interpreted as two axial rift valleys offset by about 20 km presumably by a transform zone (Berndt et al., 2016; Lonsdale & Becker, 1985, Figure 1a).

Spreading in the GB is ongoing as microseismicity beneath the trough walls, suggesting seismic release of slip along boundary faults (Reichle & Reid, 1977). The opening of the basin is thought to have started between 4 and 6 Ma ago with a spreading rate of 4.8–6 cm/yr based on the restored position of Baja California Peninsula to its former position adjacent to mainland Mexico and GPS data (Bischoff & Henyey, 1974; Hamilton, 1961; Larson et al., 1972; Lizarralde et al., 2007; Umhoefer et al., 2020).

Sedimentation in the southeastern portion is dominated by mass transport deposits and turbidites derived mainly from the Rio Mátape and Rio Yaqui rivers. By contrast, sediments in the northwestern part are mainly of hemipelagic origin (Curray et al., 1982a; Einsele & Kelts, 1982; Lizarralde et al., 2011; Teske et al., 2021a). These hemipelagic deposits are largely composed of diatoms resulting from high primary organic productivity in the photic zone (Curray et al., 1982a; Einsele & Kelts, 1982; Van Andel, 1964). Sediment accumulation rates in the GB show a wide range of values that vary between 1 and 5 m/kyr (e.g., Berndt et al., 2016; Calvert, 1966; Teske et al., 2019, 2021a), keeping the floor of the trough mostly smooth. These rates are

much greater than typical pelagic rates of 5–50 mm/kyr (Bischoff & Henyey, 1974; Calvert, 1966; Curray et al., 1982a) presently observed in the southern GOC (e.g., Ramírez-Zerpa et al., 2022), but are in line with sedimentation rates documented for the Tiburón, Wagner, and Laguna Salada basins north of GB (e.g., Aragón-Arreola & Martín-Barajas, 2007; Contreras-Pérez et al., 2012; Dorsey, 2010). Sediment thickness in the GB is in the order of 1–3 km (Lizarralde et al., 2007; Teske et al., 2021a). In fact, it is thought that the high sedimentation rates in the GB inhibit the extrusion of basalts onto the basin floor, the formation of a typical ridge axis, and the appearance of magnetic anomalies (DeMets, 1995; Klitgord et al., 1974; Lawver & Hawkins, 1978; Levi & Riddihough, 1986; MacDonald & Atwater, 1978). Instead, sills intrude into sediments and form sheet-like structures at different levels that are likely controlled by a mechanical stratigraphy (Einsele et al., 1980; Einsele & Kelts, 1982; Kastner, 1982).

2.1 | Ringvent site

One important target of IODP Expedition 385 is Ringvent (Figure 1b). This structure consists of a circular array of active seafloor hydrothermal vents located ca. 28 km northwest of the northern trough (Figure 1b). A detailed description of the Ringvent site can be found in Teske et al. (2019) as well as Teske et al. (2021e) and is briefly summarized here. This ring-shaped structure has a diameter of approximately 800 m and rises about 15–20 m above the surrounding seafloor. It is situated on top of a cone-sheet intrusion (i.e., a saucer-shaped sill without the inner flat portion) located at a depth of around 150 m below the basin floor (Figures 1b and 3). Seismic stratigraphy reveals Ringvent is significantly younger than the crustal age (ca. 0.9 Ma) suggesting that the sills intruded off-axis (Lizarralde et al., 2011). Teske et al. (2019) found that the structure is characterized by high thermal gradient anomalies (around 5°C/m), localized hydrothermal fluid flow, methane seepage, and extensive seep fauna and microbial communities. These authors concluded that Ringvent is in transition from sill-driven hydrothermalism to cooling dominated by localized fluid flow. During IODP Expedition 385 a total of ten holes were drilled, eight along a transect from SW–NE and two (U1548D-E) in the near vicinity (ca. 1 km) of Ringvent (Figure 1b). Both holes, U1548D-E, were drilled to characterise the geochemical signature of an observed lateral change in sediment strata which may be related to the sill intrusion at Ringvent (Teske et al., 2021e).

2.2 | Previous heat flow surveys and hydrothermal circulation in GB

The first heat flow measurements in the GOC and GB were performed in the early 1960s and 1970s by Von Herzen (1963), Lawver et al. (1973, 1975), Lawver and Williams (1979), and Williams et al. (1979). They were followed by more detailed surveys in the northern and southern troughs and by DSDP Leg 64 (Curray et al., 1982a, 1982b; Fisher & Becker, 1991; Lonsdale & Becker, 1985, Table S3). The bulk of heat flow data in the GB is concentrated in and around the northern and southern troughs (Figure 1a). High values of heat flow in those areas have been interpreted as upwelling of hydrothermal waters discharging along permeable pathways such as fault zones and fissures in proximity of mafic intrusions, whereas low values of heat flow have been interpreted in terms of bottom water recharging of the hydrothermal system (Fisher & Becker, 1991; Geilert et al., 2018; Lonsdale & Becker, 1985). In the southern portion of the northern trough, heat flow sites are more scattered than in the southern trough and high heat flow zones are smaller and more isolated (Fisher & Becker, 1991, Figure 1a). Overall, low values of ca. 150 mW/m^2 are observed in the northern part of the northern trough close to the transform fault (Figure 1a). Values in the southern part of the northern trough are more sparsely distributed and high heat flow zones tend to be smaller than those in the northern part (Fisher & Becker, 1991). Existing heat flow data in the southern trough (e.g., Fisher & Becker, 1991; Lawver et al., 1975; Lawver & Williams, 1979; Williams et al., 1979) shows that the GB is associated with relatively high heat flow and that active hydrothermal cooling takes place in patches. Here, heat flow station values vary two orders of magnitude within a few hundred meters of each other (Fisher & Becker, 1991; Lonsdale & Becker, 1985).

Based on available data it can inferred the existence of three different hydrothermal systems in the GB (e.g., Gieskes et al., 1982; Kastner, 1982; Lonsdale & Becker, 1985): (1) short-lived activity produced by sills intruding into sediments characterised by relatively high heat flow and patchy active hydrothermal cooling; (2) fluid circulation in surface sediments above recent sill intrusions produced by the development of convective cells above the sills; and (3) deep magma reservoirs caused by adiabatic and flux melting in the rift environment which feed the sill intrusions at shallow levels.

3 | THERMAL DATA

The new dataset consists of thermal conductivity and equilibrium sediment temperature from which we estimate

the heat flow at each hole. It should be noted that we also estimated radiogenic heat production but these are negligible. Values of these estimates for each hole are presented in the Supplemental information.
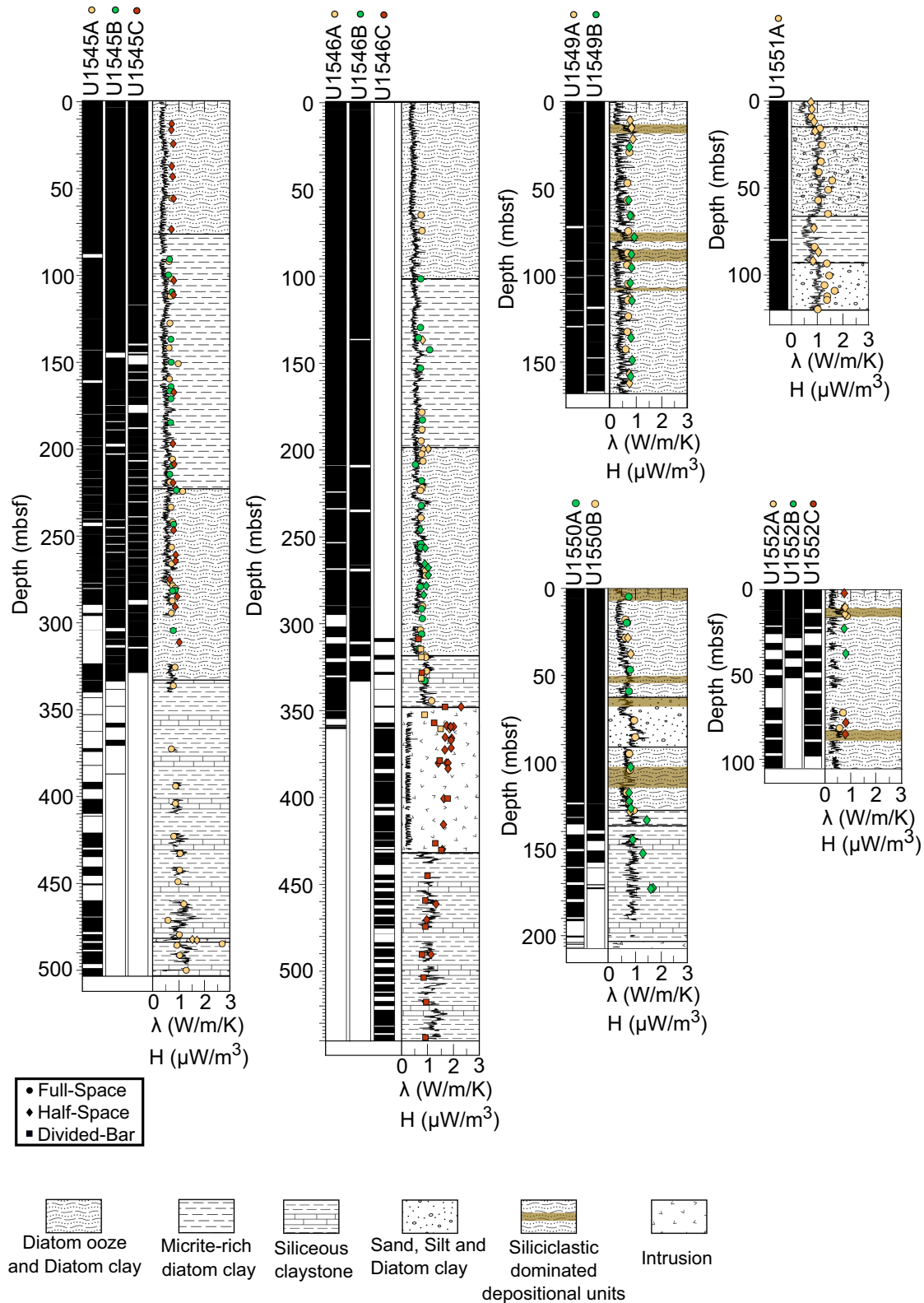
3.1 | Thermal conductivity

Thermal conductivity is an important material parameter that modulates the conductive cooling rate of sills and the transference of heat to wall rocks. This parameter was measured on recovered core material, in general on the third section of each core or neighbouring section in the case that the third section was not suitable, using both the needle probe and half-space line-source technique onboard the D/V *JOIDES Resolution* (Vacquier, 1985; Von Herzen & Maxwell, 1959). Additionally, the thermal conductivity of rock chips and some lithified sediment was measured using a divided bar apparatus which is often used for small samples of odd sizes and shapes (Beck, 1988; Crowell & Gosnold, 2012; Sass et al., 1984). In general, needle probe measurements were made in unlithified sediments, whereas half-space line-source measurements were made in lithified sediment and hard rock samples where pieces were large enough for the half-space line-source. Both techniques estimate the thermal conductivity by measuring the temperature change as a function of time during a period of transient heating. Usually, these methods yield conductivities that agree with each other within 5% or better. Additional details on these systems and the measuring procedure are given in Teske et al. (2021b). Recovered rock chips that were too lithified for the needle probe and too small for the half-space technique were measured using a divided bar technique. As described in the Supplementary Information 20 determinations of thermal conductivity using that method (Table S1 and Figure 2) were performed on samples from Site U1546, where a 77 m thick sill was penetrated. The measurements include the altered and indurated sediments above and below sill/ sediment contact zones. Thermal conductivity measurements for samples collected at similar depths (within ca. 0.5 m of each other) for the same hole but performed using half-space line-source measurements show that the lower divided bar underestimates thermal conductivity by around 16% with respect to the half-space method (Figure 2).

Thermal conductivity values were corrected for in-situ pressure and temperature conditions, assuming hydrostatic pressure and the observed background thermal gradient. We applied a pressure correction of +1% per 1800 m (Ratcliffe, 1960). Temperature affects the thermal conductivity in two opposing ways. The thermal conductivity of water filling porosity increases with temperature (Keenan et al., 1978) and thermal conductivity of the rock matrix decreases with temperature (Zoth & Haenel, 1988). We accounted for these effects by applying a temperature correction of +1% per +20°C difference between the laboratory and in situ conditions (Ratcliffe, 1960).

Figures 2 and 3 display thermal conductivity values along with major lithostratigraphic units for the drilled sites. In general, thermal conductivity varies as a function of lithology and porosity (see Figures S1A and S1B in the Supplemental Information). Thermal conductivity is relatively constant throughout the diatom ooze/clay, micrite-rich diatom clay and siliciclastic-dominated depositional units with mean and standard deviation value of 0.81 ± 0.14 W/m/K (Figure S1A). Siliceous claystone has a higher mean and standard deviation of 1.11 ± 0.42 W/m/K. The sand-silt layer observed at Sites U1550 and U1551 show the highest values in thermal conductivity but are less scattered with a mean and standard deviation of 1.25 ± 0.22 W/m/K. Because drilling-induced fractures normally broke up cores around sill-sediment contact zones (e.g., U1545 & U1546, Figure 2), only a few measurements were obtained using the divided-bar apparatus. Still, the apparatus yielded values of thermal conductivity consistent with those obtained using the needle probe and half space technique as can be appreciated in Site U1546 (Figure 2). Notice in this figure how the divided-apparatus measurements follow the shipboard estimation trend, having small discrepancies of 0.1 ± 0.07 W/m/K and 0.38 ± 0.05 W/m/K for measurements above and below the sill, respectively.

Generally, sediments display higher thermal conductivities around sill-sediment contact zones (e.g., U1545 & U1546, Figure 2) due to a reduction in porous space by ca. 50%. For the upper and lower sill/sediment contacts, offsets are 0.59 and 0.04 W/m/K, respectively. Samples from the sill intrusion show a mean offset of 0.35 ± 0.24 W/m/K between both techniques. At Site U1546, thermal conductivity increases significantly from the siliceous claystone above the intrusion (0.90 ± 0.15 W/m/K) to the sediment/ sill boundary to a mean value of 1.63 ± 0.71 W/m/K. Within the sill, conductivity values are 1.72 ± 0.21 W/m/K and decrease below the sill to a mean value of 0.99 ± 0.16 W/m/K. Sill thermal conductivities range from 1.2 to 2.0 W/m/K and are in good agreement with values for basalt published in the literature (e.g., Čermák & Rybach, 1982; Raznjevic, 1976). Samples recovered from the sill layers showed alterations near the contact zones, moderate vesicularity with rounded inclusions and a transition from fine to medium up to coarse-grained textures towards the centre of the sill. These factors can contribute to the observed variation in thermal conductivities.

FIGURE 2 Generalized lithology of the Guaymas Basin drilling sites with thermal conductivity λ (W/m/K) (colours and symbols represent different holes and measuring technique, respectively) and radiogenic heat production H ($\mu W/m^3$) (solid lines). Radiogenic heat production is shown from the deepest hole at each site, in the case of U1546 a combination of hole A and hole C. Core recovery is shown to the left of each plot.
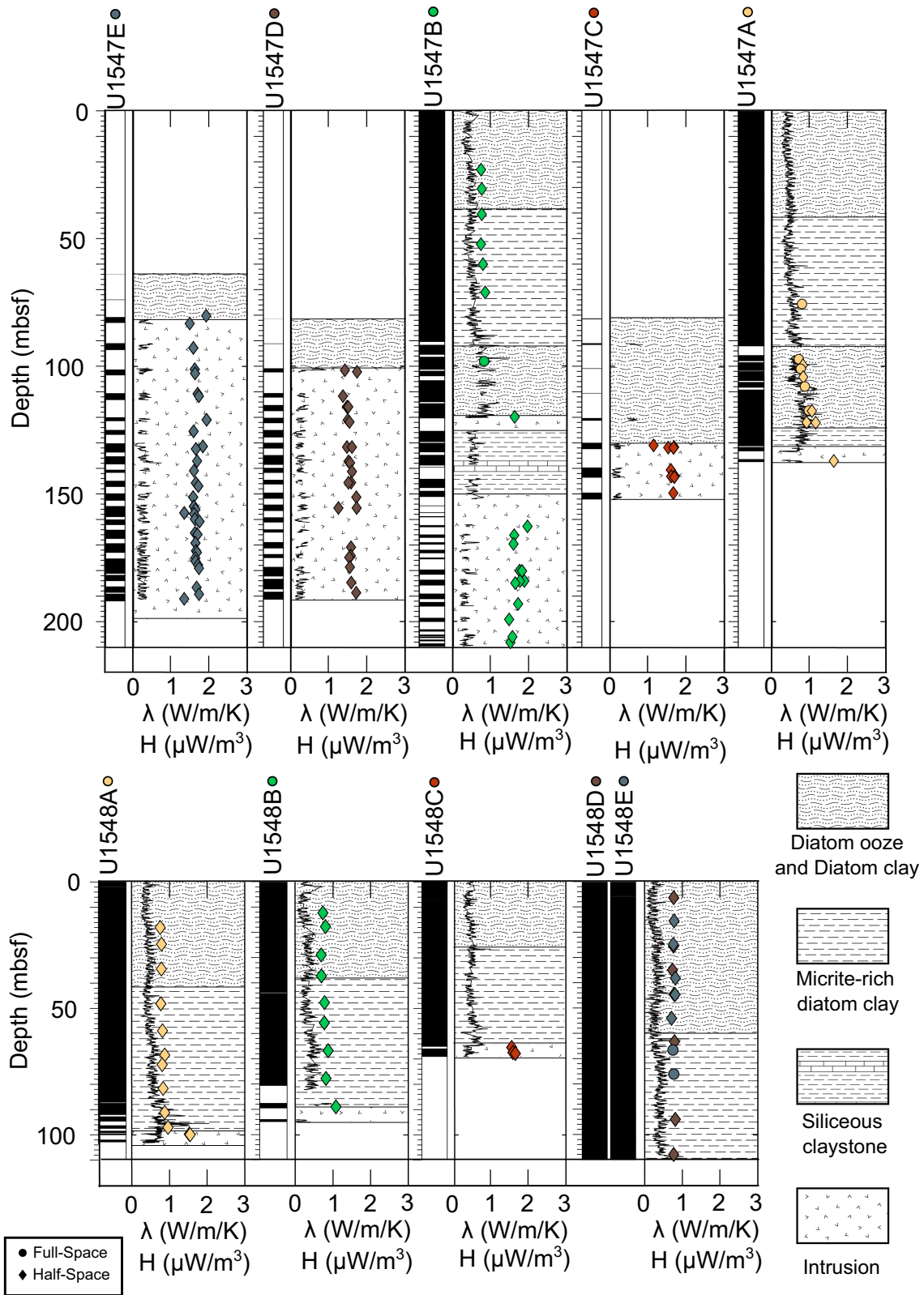
FIGURE 3 Generalized lithology of the Ringvent drilling sites with thermal conductivity λ (W/m/K) (colours and symbols represent different holes and measuring technique, respectively) and radiogenic heat production H (μW/m³) (solid lines). Core recovery is shown to the left of each plot.

3.2 | Downhole temperature measurements

A total of ninety-three high-quality in-situ temperature measurements were made in the GB (Figure 4 and Table 1). Downhole equilibrium temperatures were measured with the Advanced Piston Corer Temperature Tool (APCT-3, Heesemann et al., 2006), which is depoyed on a core barrel, and the Sediment Temperature Tool (SET-2) that fits within the cutting shoe of the Extended Core Barrel (XCB) coring tool. The SET-2 was designed for measuring temperatures in semi-consolidated sediments too stiff for the APCT-3 tool (Davis et al., 1997). During Expedition 385, we used two sets of the APCT-3 and SET-2 tools. The first set was calibrated up to a temperature of 55°C,

while the second set was accurate up to 90°C (Teske et al., 2021b). To avoid thermal disturbance from drilling, the APC is hydraulically advanced 9.5 m into the sediment beyond the drill bit at the bottom of the hole. The APCT-3 is then held in position for 7 to 10 min while the frictional heating of penetration decays and temperature is recorded as a function of time. The temperature–time series is then extrapolated to equilibrium sediment temperatures by fitting synthetic curves to the recorded data. In stiffer and more lithified sediments, the SET-2 tool is used, but it only penetrates 1.4 m below the drill bit and is held in place by applying weight. A drawback of the more lithified sediments is that cracks can develop during the tool insertion, degrading the quality of the temperature measurement. Poor SET-2 measurements occurred six out of the 93
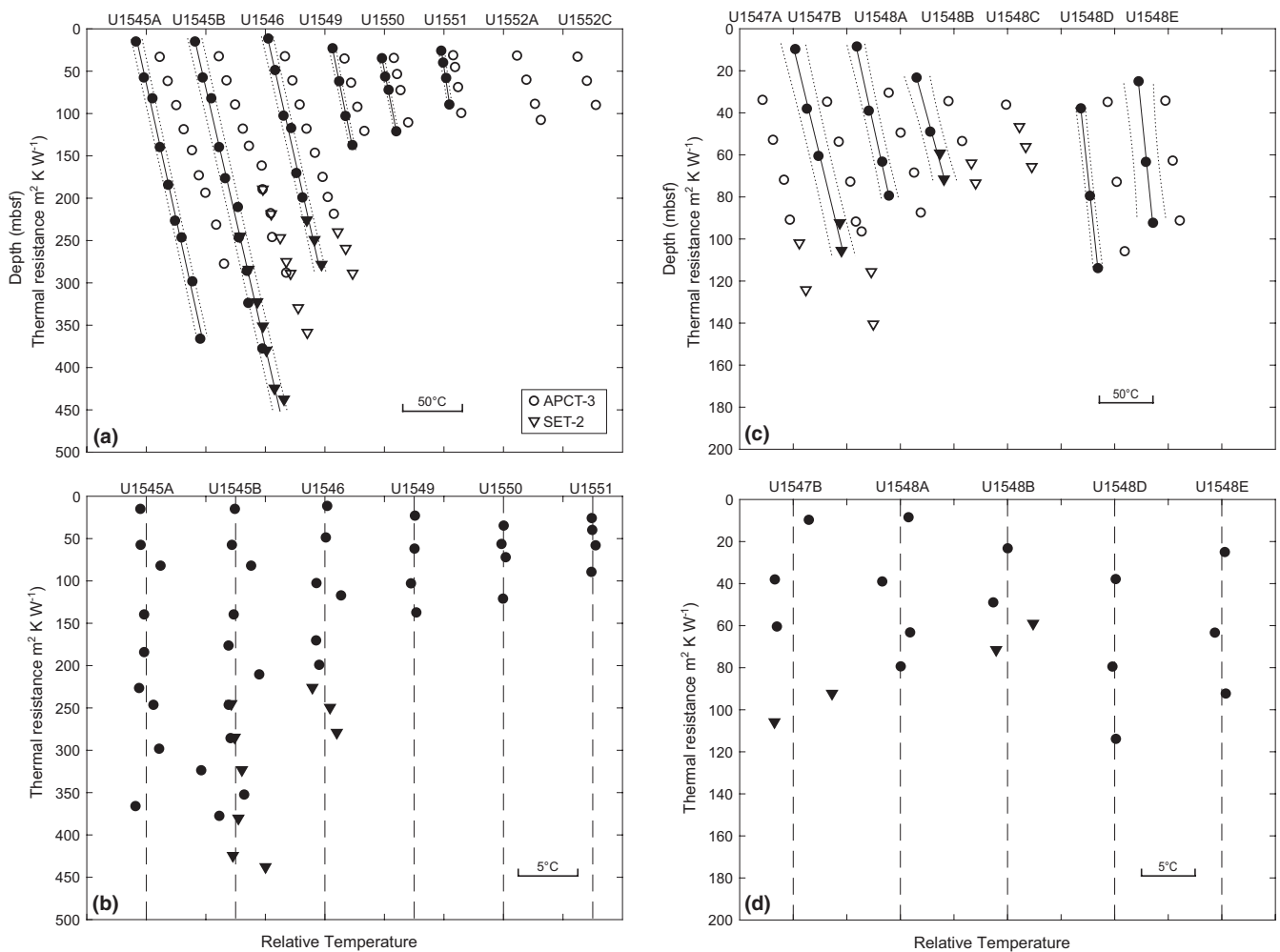
FIGURE 4 Equilibrium sediment temperature measurements and heat flow analysis for IODP Expedition 385 presented for Guaymas Basin (a, b) and Ringvent (c, d) sites. APCT-3 and SET-2 instruments are plotted as circles and squares, respectively (a, c). Temperature plotted as a function of depth (open symbols) and to the left the corresponding cumulative thermal resistance (solid symbols). Solid line shows best-fitting linear fit and the slope indicates the heat flow (q) and the intercept is the long-term bottom water temperature (T_0, Table 1). Dotted lines indicate 95% confidence interval from the linear fit. (b, d) Residuals from the linear fit plotted as a function of thermal resistance. Symbols are plotted on a relative scale to avoid overlap and the dashed line shows position of residual for each site. Note that, for U1547B only 5 temperatures with their respective thermal resistance are shown.

times and these outlier measurements are excluded and not discussed.

Most holes have 3–5 equilibrium temperature measurements (Figure 4 and Table 1). Site U1545 has the most, with a total of 30 measurements. Measurement depth ranges from ~30 mbsf at U1548 to ~359 mbsf at Site U1545, with most measurements between 65 and 120 mbsf. Thermal gradients range from 100°C/km at the eastern side of GB (U1550) to 958°C/km at Ringvent (U1548).

3.3 | Heat flow determinations

Heat flow was calculated using the thermal resistance method (Bullard plot, Bullard, 1939), which allows the calculation of heat flow even if thermal conductivity changes with depth. This method includes only thermal conductivity measurements within the depth range of the temperature measurements and assumes that heat flow remains constant with depth; this makes possible to express variations in temperature $T(z)$ with depth, z, as a function of cumulative thermal resistance $1/\lambda(z)$ as described by Equation (1):

$$T(z) = T_0 + q_0 \sum_{i=1}^{N} \Delta z_i / \lambda(z)_i. \tag{1}$$

Here T_0 is the long-term bottom water temperature, q_o is surface heat flow, $\lambda(z)_i$ is the thermal conductivity measured over the ith depth interval, Δz_i, and the summation is performed over N depth intervals from the surface to the depth of interest z_N. In practice, $T(z)$ is plotted as a function of summed thermal resistance, and T_0 and q_0 are estimated through a least square fitting algorithm (Figure 4a,c). However, at four holes (U1547A, U1548C, U1552A, and U1552C), only a handful of thermal conductivities were measured and therefore, heat flow was estimated using Fourier's law,

$$q_0 = -\lambda \, \mathrm{d}T / \mathrm{d}z. \tag{2}$$

The resulting heat flow values and uncertainties for each hole are listed in Table 1; uncertainties were computed using: (1) standard deviation from the 95% confidence interval of the linear regression to the Bullard plot (Figure 4); and (2) the error propagation using the variance formula (Equation 4, Supplemental information). The latter was used for those cases where Fourier's Law was applied and included uncertainties for thermal conductivity and gradients. In general, the total uncertainties are about 18% of the heat flow magnitude.

Heat flow from the drilled sites in the GB shows high variability with values ranging from 108 to 929 mW/m² (Figure 1 and Table 1). The highest heat flow is observed at Ringvent Site U1547 where 5 holes were drilled. The mean and standard deviation values within the ring structure are 548 ± 30 mW/m². Holes U1548A, B, and C approach the outer rim of the structure, and show increasing heat flow values from 516 to 929 mW/m² with a mean and standard deviation value of 697 ± 211 mW/m². At about 1 km distance from Ringvent, Holes U1548D and U1548E show similar heat flow values of around 251 ± 30 and 238 ± 108 mW/m², respectively. The most northwestern Sites U1545 and U1546 have consistent values of ca. 160 mW/m². These two sites contain the thickest and most complete stratigraphic record of the basin. Site U1545 was selected to provide a reference sedimentary succession not thermally altered to compare with Site U1546 which has a significant degree of alteration from sill intrusions (Teske et al., 2021a). Site U1552 located northeast of the Ringvent site, towards the Sonoran margin, shows a slightly higher heat flow of about 200 mW/m². At this site, hydrate-rich sediments overlying the sill intrusion at a depth of approximatly 700 m below the basin floor (Teske et al., 2021i) expanded in the core liner and complicated shipboard thermal conductivity measurements. The uncertainties associated with these effects are difficult to account for and the heat flow estimate for this site should be interpreted cautiously. Site U1549 targeted an off-axis seep characterised by a loss in seismic coherence, suggesting gas upflow (Teske et al., 2018, 2021f). The observed heat flow at this site is 144 ± 16 mW/m² but gas expansion, once again, made needle probe measurements inaccurate, forcing us to use the half-space line-source method instead. Heat flow decreases to a value of 141 ± 17 mW/m² at the axis of the northern trough (U1550, Teske et al., 2021g). However, the lowest heat flow value recorded (108 ± 24 mW/m²) is at Site U1551 located in the southeastern GB. At this site a cone-sheet sill intruded into terrigenous turbidite sediments (Teske et al., 2021h).

4 | DISCUSSION

4.1 | Conductive cooling

Figure 5 illustrates heat flow data compiled for the GB (Table S3) displayed as a function of crustal age assuming a constant full spreading rate of 50 mm/yr (Lizarralde et al., 2011; Umhoefer et al., 2020). The thermal structure of normal oceanic lithosphere is well described by plate

TABLE 1 Thermal analysis summary of the drilled sites.

Site	Latitude (°)	Longitude (°)	Seafloor depth (m)	$\Gamma \pm \sigma_\Gamma$ (°C\km)	$\lambda \pm \sigma_\lambda$ (W/m/K)	Number of temperature measurements	Depth range of temperature measurements (mbsf)	$q \pm \sigma_q$ (mW/ m²)	T_0 (°C)
U1545A	27.6372	−111.8890	−1593.5	228 ± 11	0.88 ± 0.35	13[a]	33.0–498.6[a]	156 ± 9	9.9
U1545B	27.6372	−111.8888	−1594.2	224 ± 10	0.88 ± 0.36	17	32.2–358.6	163 ± 9	8.6
U1546A	27.6314	−111.8799	−1586.1	221 ± 5	1.10 ± 0.44	12[b]	32.3–323.0	160 ± 13	20.2
U1549A	27.4722	−111.4797	−1840.6	194 ± 8	0.78 ± 0.08	4	35.0–120.5	144 ± 16	6.7
U1550A	27.2527	−111.5069	−2001.0	159 ± 14	0.92 ± 0.28	5[c]	34.3–125.4	141 ± 17	3.0
U1551A	27.2065	−111.2199	−1844.0	100 ± 12	1.14 ± 0.28	4	31.1–99.3	108 ± 24	5.1
U1552A	27.5548	−111.5494	−1841.6	262 ± 10	0.76 ± 0.08	4	31.5–107.5	199 ± 18[d]	–
U1552C	27.5536	−111.5476	−1844.3	269 ± 18	0.76 ± 0.09	3	32.8–89.8	205 ± 26[d]	–
Ringvent sites									
U1547A	27.5076	−111.6783	−1733.7	544 ± 65	0.97 ± 0.26	5	33.8–124.2	528 ± 155[d]	–
U1547B	27.5069	−111.6789	−1732.2	506 ± 135	1.40 ± 0.45	4	34.7–140.5	570 ± 84	21.0
U1548A	27.5041	−111.6811	−1739.9	646 ± 175	0.94 ± 0.28	4	30.4–87.4	516 ± 80	21.9
U1548B	27.5042	−111.6810	−1738.9	804 ± 151	0.80 ± 0.12	4	34.4–73.4	646 ± 168	18.9
U1548C	27.5045	−111.6808	−1737.0	958 ± 365	0.97 ± 0.33	4	36.1–65.6	929 ± 475[d]	–
U1548D	27.5089	−111.6898	−1729.3	268 ± 8	0.78 ± 0.04[e]	3	34.8–105.8	251 ± 30	2.6
U1548E	27.5081	−111.6882	−1729.9	283 ± 18	0.78 ± 0.04[e]	3	34.2–91.2	238 ± 106	6.4

Note: [a]SET-2 measurements for Hole U1545A are excluded from the thermal analysis. [b]Last SET-2 measurement for Hole U1546A is excluded from the thermal analysis. [c]SET-2 measurement of Hole U1550A is excluded from the thermal analysis. [d]Heat flow estimated using Fourier's law; Error calculated using Variance formula. [e]Thermal conductivity calculated from both holes, U1548D, E.
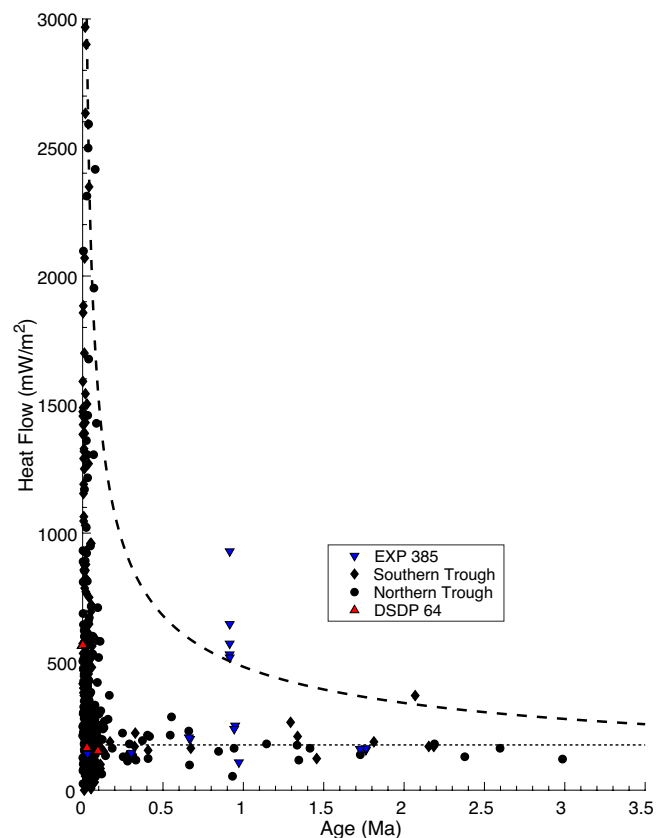
FIGURE 5 Compiled heat flow data from the Guaymas Basin as a function of plate age. Shallow heat flow probe measurements are separated for the northern (circles) and southern (diamonds) troughs; blue and red symbols represent IODP and DSDP expeditions, respectively. Dashed lines show the conductive cooling model (wide) and the linear trend after ca. 0.2 Ma (slim).

spreading models that show a scaling relation $q \sim t^{-1/2}$ between heat flow, q, and plate age, t, for seafloor ages >50 Ma (e.g., Goutorbe, 2010; Stein & Stein, 1992). This cooling trend corresponds to the dotted line in Figure 5 and is shown as reference. Heat flow values in the GB correspond to plate ages <3 Ma, with the majority of estimates <0.5 Ma because the objective of those surveys was to understand the northern and southern troughs. Low values for young crustal ages are located around nearby normal faults and are interpreted to be sites of bottom water recharge (Fisher & Becker, 1991). High heat flow values ≥600 mW/m² are associated with shallow sill intrusion, while areas with values ≥1000 mW/m² are associated with hydrothermal edifices (Lonsdale & Becker, 1985; Fisher & Becker, 1991; Geilert et al., 2018; Figures 1a and 5). Finally, values >1500 mW/m² are in good agreement with conductive values predicted from the half space cooling model of mid-ocean ridges (e.g., Hasterok, 2013; Parsons & Sclater, 1977; Stein & Stein, 1994; Figure 5). However, a word of caution: heat flow variability at the GB is almost certainly the result of

ongoing sill intrusions in which hydrothermal circulation has little or no influence on how heat is dissipated within the lithosphere (Fisher, 1998).

Excluding values close to the troughs, we estimate heat flow in the GB to be $176 \pm 48 \, \text{mW/m}^2$. This is essentially the same value estimated by Lawver and Williams (1979) of $180 \pm 10 \, \text{mW/m}^2$. Either way, these values are lower than those predicted by conductive cooling models (Figure 5). Heat flow values for crustal ages >=0.2 Ma also display reduced variability, indicating a regional background thermal regime.

It is noteworthy that none of the heat flow values discussed above are corrected for perturbations associated with bottom water temperature variations and thermal refraction. These effects are negligible (see Supplementary Information). In contrast, the influx of sediment which transiently decreases temperature until the deposited sediment warms to the background thermal regime, can be an important effect but variations and poor knowledge of sediment accumulation rates around the GB make it difficult to determine precise values for this correction. The only area with reliable information is the northern edge of the basin. Two sites there show sediment accumulation rates of 364 m/Ma (U1552) and 1020 m/Ma (U1545/1546). Although these rates are enough to decrease heat flow by 8% and 20%, respectively (see Figure S2 and Table S2 in Supplemental Information), they appear to be on the low side. For example, heat suppression in the Wagner Basin in the northern GOC, whose tectonostratigraphy might be analogous to the central GB, can be as high as 50% (Neumann et al., 2017; Peña-Domínguez et al., 2022). In either case, the corrected heat flow would still be lower than that predicted by the cooling model.

## 4.2 | Influence of transform faults on the regional thermal regime

In the previous section we compared the GB with a one-dimensional purely conductive lithospheric cooling model. This assumption is partially incorrect as the GB is also bounded by two transform faults: the Canal de Ballenas and Farallon Transforms that link GB with the Delfín and Farallon basins to the north and south, respectively (Figure 1a). In addition, the GB troughs are offset by a central transform around 20 km long. We now compare the thermal influence of the transform/fracture zones that enclose the basin and dissect the central trough with idealized thermal models of oceanic ridge-transform-ridge systems (e.g., Chen, 1988; Forsyth & Wilson, 1984; Lonsdale, 1989; Louden & Forsyth, 1976; Morgan & Forsyth, 1988). In these models plates are initially in thermal disequilibrium causing a significant exchange of heat

across transforms that gradually diminishes with distance and age as plates reach thermal equilibrium (Louden & Forsyth, 1976). However, the tectonic configuration of the GB central troughs is distinct from that anticipated by models as both troughs display significant overlap. The age offset in the eastern part of the southern trough, between the younger (southern) and the older (northern) plate, is around 0.3 Ma, significantly smaller than the one used in numerical setups (Forsyth & Wilson, 1984; Louden & Forsyth, 1976).

To avoid the high variability close to the troughs, we only present heat flow data for plate ages >=0.5 Ma in two q vs. distance-to-transform diagrams (Figure 6). Each datum in these diagrams has been colour-coded with its plate age. It is also noted that only a few measurements are available to test some of the model's predictions. We chose four profiles across the fracture zone with different age offsets (Figures 1a and 6b). The profiles shown in Figure 6b display values of 159 ± 6 and 177 ± 46 mW/ m^2 for the southern and northern part of the transform segment, respectively (Figure 1a). Heat flow values for the younger plate generally exceed models' predictions though no conclusive statement can be made based on the limited heat flow measurements available across the fracture zone

and the fact that values are within one standard deviation (Figure 6b). In Figure 6, it can also be observed that: (1) no clear relation exists between heat flow and distance-to-transforms; (2) the same is true for heat flow and plate age; (3) both proximal heat flow values (<8 km) and distal ones (>30 km) show steady values of 140 mW/m^2, less than the estimated average heat flow of ca. 175 mW/m^2; and (4) there is a slight rise in heat flow at a distance of around 20 km from the faults but the dataset cannot fully resolve whether the transforms are the source of these anomalous values or a high heat flow anomaly parallel to the northern transform fault.

Our conclusion is that even though the GOC's oblique motion is organized by several en-echelon transform faults connected by a series of pull-apart basins, in the GB, these structures appear to have little influence. Instead, most of the heat is dissipated by two thermal regimes. A thermal regime within the northern and southern troughs characterized by heat advection due to magmatic intrusions and hydrothermal circulation from adiabatic and flux melting at the base of the crust. Heat flow in the troughs can reach values of ca. 1 W/m^2 though it is highly variable and influenced by the presence of bottom water recharge and hydrothermal discharge zones. The heat collected at the
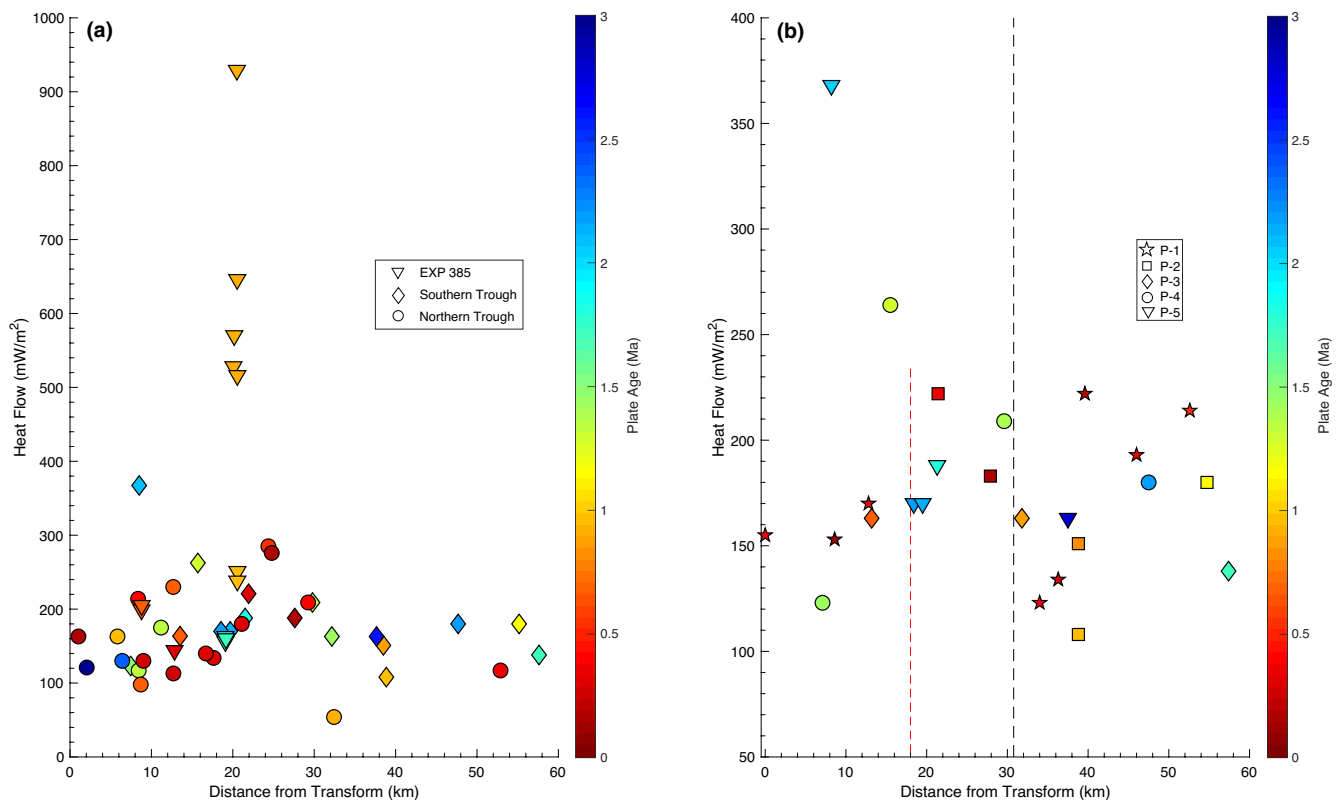
FIGURE 6 Comparison between heat flow, distance to the transform faults, and plate age (Figure 1). (a) Heat flow plotted against the distance to the transform fault for the respective troughs (circles and diamonds). Expedition 385 drilling sites are represented in triangles. (b) Heat flow as a function of distance from the fracture zone in the southern trough (Figure 1). Symbols correspond to boxes shown in Figure 1 and dashed lines show the location of the central transform fault (red) and fracture zone (black) illustrated in Figure 1a.

troughs is rapidly dissipated to steady conditions of ca. 180 mW/m² for plate ages >0.2 Ma with isolated patches of anomalous heat flow, corresponding to young, off-axis sill intrusions that can release heat at about 500 mW/m² (e.g., Ringvent; Figure 5). These intrusions, however, cool off at timescales of a few tens of thousands years and cannot explain the steady heat loss observed throughout the basin. This "background" heat flow is likely the product of the slow release of latent heat by the formation of new gabbroic crust below the sediment cover and the narrow thickness of the newly formed crust (ca. 6 km, Lizarralde et al., 2007). In addition, some degree of thermal homogenization is expected similar to what is observed in the Middle Valley, where comparable amounts of conductive and convective fluxes of roughly about 1 W/m² is distributed equally in an area of 260 km² (Stein & Fisher, 2001).

4.3 | Hydrothermal activity at Ringvent

We explore in more detail systematic variations in superficial mass and energy fluxes that control the development of microbial colonies and spread of chemical alteration of organic-matter rich sediments around sills. These fluxes in conjunction with the cooling time scale are limiting factors in the production of hydrocarbons in the GB. Calibration of thermokinetic models looking to assess the generation of greenhouse gasses by the transformation of organic matter rely on those boundary conditions as well (e.g., Aarnes et al., 2010; Galerne & Hasenclever, 2019).

We fitted an analytical solution of the one-dimensional advection–diffusion equation by Darcy flow, to the temperatures measured at Ringvent using a grid search method (Bredehoeft & Papaopulos, 1965; Supplemental information). The best fitting Darcy velocity was chosen by minimizing the RMS error between the observed and modelled downhole temperature (Figure 7). The reference system in this figure is oriented downwards; thus, negative Darcy velocities denote upflow. From the best fitting solution, we also identified sites of superficial discharge and recharge from the curvature of the temperature-depth profiles. Discharge induces curvature at the top of the convecting layer while recharging at the base. For example, it is possible to tell hole U1548C in Figure 4c is a discharge site by the way in which the thermal gradient is curved.

Discharge flow is maximum in Hole U1548C close to the edge of the sill (−202 mm/yr) and minimum in Hole U1548D (−11 mm/yr), approximately 700 m away from the sill. Notice that hole U1548D shows a slight positive velocity within the range of uncertainties indicating a rather weak recharging zone. In addition, Figure 7 shows that heat flow and fluid discharge are related in a reciprocal manner. As discharge velocities decrease, there is less
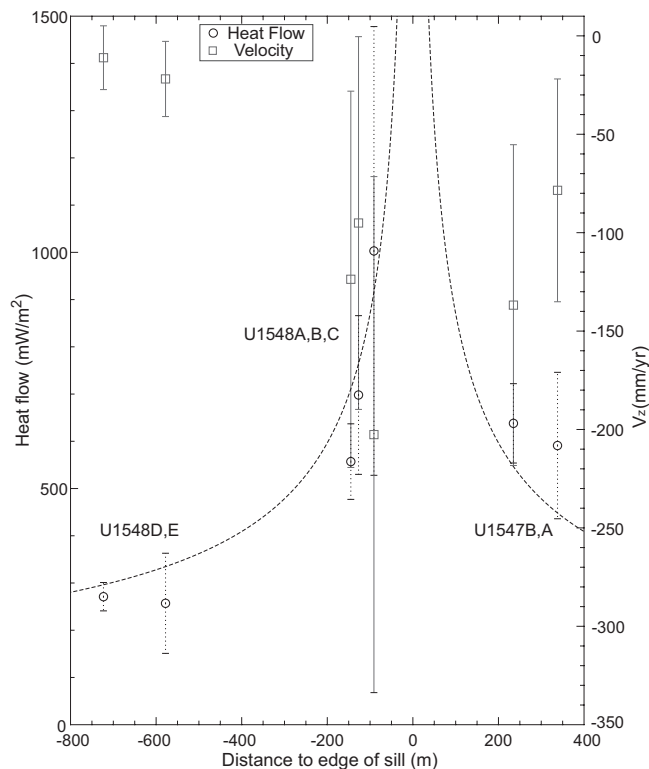

FIGURE 7 Heat flow and discharge velocities with their respective standard deviations as a function of distance to the edge of the sill intrusion at the Ringvent sites.

hydrothermal circulation carrying away heat. As a result, heat flow decays with an inverse square root from a value of ca. 1000 mW/m², at the edge of the cone-sheet intrusion, to approximately 200 mW/m², 700 m from the sill's edge (Figure 7).

The fluxes described above demonstrate hydrothermal circulation infiltrates an area of approximatly 2 km in diameter or roughly three times the diameter of the structure (750 m). The average heat flow within this zone is 574 mW/m² with a mean discharge of ca. 127 mm/yr. Fisher and Becker (1991) estimated the heat output in the southern trough to be ca. 5×10^7 to 4×10^8 W and calculated a steady-state thickness of the intruded layer of ca. 200 m using an average heat flow of 450 mW/m² (see fig. 10 in Fisher & Becker, 1991). The updated figures for Ringvent provide a more precise value of 240 ± 115 m, for the thickness of the layer, and a heat output of ca. 10^7 - 2×10^7 W. This is a small fraction of the energy released by diking in mid ocean environments (ca. 1 GW/km) and is on par with the output of a single hydrothermal vent (Fisher & Becker, 1991).

Superimposed on the long-term conductive cooling, sills lose heat by advection of heat. According to Galerne and Hasenclever (2019), the later mechanism is dominant only during an initial period lasting a few thousand years of cooling by hydrothermal circulation. Ringvent sites

currently show a strong correlation between heat flow and the thickness of sediment overlying the sill intrusion, suggesting that the phase of rapid cooling is over and, at most, residual amounts of heat are being transferred advectively (Figure 3). Sediment thickness for holes U1548A-C varies between 66 and 98 m and extrapolated sediment-sill interface temperatures vary between 61 and 73°C. Such a temperature range may represent the temperature of the upper part of the hydrothermal system as it matches quite well with the temperature of hydrothermal hot spots at Ringvent (75°C). The product of this temperature, appropriate values of heat capacity (ca. 1 kJ/kg C) and density of water (1000 kg/m^3), and our average Darcy flow rate, gives an estimate of the energy density transported by hydrothermal circulation at Ringvent, which is in the order of 90 mW/m^2. This is a small fraction of the conductive heat loss that proves Ringvent is in a weak hydrothermal circulation state approaching equilibrium with the surrounding sediments.

Sedimentation rate at Ringvent is ca. 500 m/Ma (Geilert et al., 2018; Teske et al., 2021e). With a sediment cover between 60 and 120 m at the edge and the centre of the conic sheet intrusion, respectively (Figure 3), that rate yields a maximum age estimate of sill emplacement of 120–240 kyr. The conic sheet intrusion, however, must be considerably younger than those ages given the presence of abundant calcite-filled cracks and peperite breccia in the cores above the sill (Teske et al., 2021e). The absence of pillow lavas in the cores further supports the conclusion that the sill intruded into fluid-saturated, unconsolidated sediments (Teske et al., 2021e). Geilert et al. (2018) estimated from ceased fluid mobilization, an age of 3–24 kyr; however, our new data can safely dismiss the lower bound estimate given the weak convective regime currently observed. If this is the case, the time scale τ of conductive cooling of the instantaneous heating of a body can be determined by using a distance r where steady-state is assumed (i.e., the water/sediment interface) and the thermal diffusivity κ, of the sediments given by the product $\kappa = \lambda / c_v \rho$. τ, r, and κ are related to each other through the relation $\tau = r^2/\kappa$. Assuming a typical value for the thermal diffusivity of 5×10^{-7} m^2/s for the fine-grained sediments of GB (e.g., Fuchs et al., 2015; Goto & Matsubayashi, 2009) and a characteristic length of $r = 210 \pm 88$ m (burial depth plus half the sill thickness), leads to an estimate age of emplacement in the range of 5–28 kyr.

4.4 | Thermal structure of the Guaymas Basin and magma production

Our new measurements may have some bearing on the question of what thermal processes enable rifting in

non-volcanic, sediment-filled rifts like the central and northern GOC. Lizarralde et al. (2007) and other authors have speculated that the copious sedimentation in GB behaves as a thermal insulator causing the continental crust to warm thereby facilitating rifting. It has been by now well established (e.g., Bialas & Buck, 2009) that indeed rifting style varies in complex ways as a function of sedimentation rate, but not as anticipated in the early studies. Numerical models carried out by Bialas and Buck (2009) demonstrated that sediment blanketing actually cools the lithosphere, which results in an overall strengthening effect.

We explore the idea that a relatively small volume of magma supplied by flux melting in a narrow rift may provide sufficient heat to weaken the upper crust (Bialas et al., 2010). As a first approach, we consider the simple conceptual model depicted in Figure 8, which shows a control volume in the zone of active sill emplacement in the GB troughs. In this model, we devise a basal layer approximatly 6 km thick (Lizarralde et al., 2007) made from gabbroic rocks and dehydrated greenschist/amphibolite facies metasediments (e.g., Christensen & Salisbury, 1975; Rangin et al., 1983; Stern et al., 1976). Thanks to their high
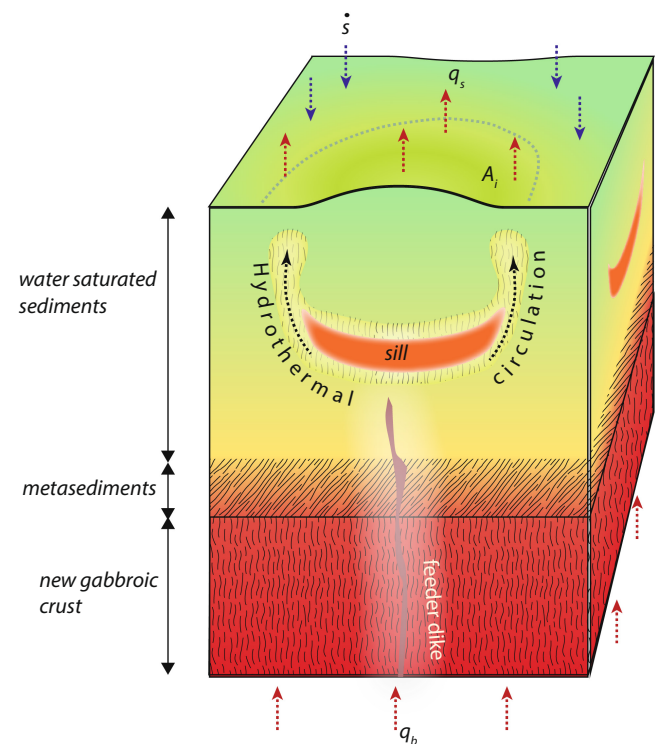

FIGURE 8 Representative volume of the Guaymas Basin, central Gulf of California. The elements contained in the control volume govern the thermal evolution of the basin at different time scales according to the balance of heat discussed in the main text. q_b is the basal (background) heat flow; q_s is the superficial heat flow; $\dot{s}$ represents the rate at which new mass enters the reference volume; A_i is the area of the sill.

thermal conductivities, these rocks draw heat from the emplacement of hot grabboic material at the base of the crust and the slow release of latent heat by crystallization. As the control volume moves away from the rift axis by the divergent plate motion, the low conductivity and permeability layer cools off, perhaps punctuated by the occasional intrusion of new sills such as at Ringvent.

This primary system, dominated by conduction of heat, is overlain by a layer 1–3 km thick of sediments (Lizarralde et al., 2007), consisting of a mixture of water-saturated fine-grained hemipelagic and turbidite deposits of low thermal conductivity and permeability. Moreover, those sediments often display a mechanical layering and fracture stratigraphy of contrasting strength and brittleness that prevents dike intrusions to reach the surface, promoting the transference of heat from the sills to the sediments. This low thermal conductivity and permeability environment induces a second thermal regime in which hydrothermal circulation and conduction warm the upper layer from within and cause widespread alteration around the sills and feeder dikes. Thus, we expect the upper layer to undergo an initial period of transient cooling and elevated heat flow for young plate ages, followed by a long-term steady cooling regime as both layers equilibrate thermally. This first-order prediction can be readily validated in the heat flow vs. age plate profiles shown in Figure 5. This figure shows a clear changeover at ca. 200 ± 50 kyr from rapid cooling followed by equilibrium at a level of ca. 180 mW/m². Moreover, based on the thermal relaxation time, we can solve for the thickness, h, of the sediment layer using the expression $h = (\kappa \tau_c)^{1/2}$ in which $\tau_c = 200 \pm 50$ kyr is the critical changeover time. Assuming again a typical thermal diffusivity value of $\kappa = 5 \times 10^{-7}$ m²/s we obtain a thickness of the sediment layer of 1.5–2 km, which is in good agreement with the thickness estimated from velocity analysis of seismic waves (Lizarralde et al., 2007).

To better constrain the rate of magma supply and the sill intrusion interval necessary to keep the GB crust hot, we devised the following simple order of magnitude model based on the balance of energy equation:

$$\frac{dE}{dt} = Q, \tag{3}$$

where the left-hand side of Equation (3) represents the change of stored energy, E, in the control volume (Figure 8) and Q is the net flux of energy lost through the water/sediment interface. Since the deformational energy is clearly negligible, we only consider the internal energy given by the product of the mass (M) inside the control volume, its heat capacity (c_v) and the change in temperature (ΔT) produced by the intrusions: $E = M c_v \Delta T$. Similarly, Q can be expressed as the difference between the superficial heat flow density

leaving the volume, q_s, and the basal heat flow entering the volume, q_b, times the area of the sill A_s: $Q = (q_s - q_b) A_i$. Notice that the mass of the system can be expressed as the sum of the mass of the host rock, M_h, at some arbitrary time and the mass of the sills, m_i, plus the mass of sediment being incorporated to the control volume at the seafloor, m_s, that is, $M = M_h + m_i + m_s$. Substituting these relations in Equation (3) and assuming thermal steady state, we obtain the following expression for the rate of magma injection

$$\frac{\delta m_i}{\delta t} \approx \frac{A_i (q_s - q_b + \dot{s} \rho_s c_v \Delta T)}{c_v \Delta T}, \tag{4}$$

where $\dot{s}$ is the sedimentation rate and ρ_s is the density of the sediments. It should be evident that the term $\dot{s} \rho_s c_v \Delta T$ on the right-hand side of Equation (4) is the reduction in heat flow caused by sedimentation. Also notice that advection of heat is ignored as the flow velocities are too small to be applicable. In the calculations below, we have assumed a typical sill with an area of 5 km², heat capacity of roughly 1 kJ/kg C, and a characteristic temperature rise of 400°C caused by the intrusions. We also adopt a characteristic thickness of 50 m and a density of 2700 kg/m³ for the sills. In the model, the basal heat flow q_b is the average background flow of 175 mW/m² and the superficial heat flow released by sills q_s is the average heat flow of Ringvent of 575 mW/m².

According to Equation (4), to sustain a long-term average superficial heat flow of 575 mW/m², it is necessary to inject magma at a rate of ca. 15×10^7 kg/yr. This translates to approximately one sill per 1000 yr if we consider that the magma supply is episodic rather than continuous. When our model is extrapolated to the entire rift axis, it predicts a magma production rate of approximatly 10^{-2} km³/yr. The predicted frequency is remarkably similar to the interval required by numerical models to generate viable rifting solutions for the repeated dike intrusion in the continental lithosphere (Bialas & Buck, 2009). Our estimation, however, is one order of magnitude longer than the timescales of magma intrusion processes within the incipient seafloor spreading centres of the Afar rift (approximate century interval; Ebinger et al., 2010). The predicted magma production rate of ca. 10^{-2} km³/yr is also substantially lower than the average flux of approximatly 2 km³/yr documented for large igneous provinces (LIPs; Courtillot & Renne, 2003). But this comparison has obvious limitations as the formation of LIPs is often attributed to mantle plumes (e.g., Morgan, 1983; Wilson, 1997), and there is no evidence of vigorous mantle upwelling playing a role in the development of the GB or elsewhere in the gulf (Negrete-Aranda et al., 2013; Persaud et al., 2015; and references therein). Despite these differences, our simple model suggests that: (i) a relatively low rate of magma emplacement in

active continental rifts is sufficient to reduce lithospheric strength which could help trigger final continental rupture (Buiter & Torsvik, 2014); and (ii) for this to happen, intrusions must surface at shorter timescales than their characteristic cooling time of 10^4 yrs. Otherwise, all heat from a sill will be dissipated away or transported into the water column by hydrothermal circulation before the subsequent intrusion resulting in strengthening of the lithosphere (Bialas et al., 2010) on account of the large shear strength of igneous rocks.

5 | CONCLUSIONS

Based on the results of the measurements at drilling sites in the GB, we conclude the following:

1. The Northern and Southern Troughs of the GB display heat flow values >600 mW/m^2 associated with ongoing sill intrusions in the young crust in which hydrothermal circulation has little or no influence on how heat is dissipated within the lithosphere.
2. Heat flow values decay rapidly for crustal ages greater than 0.2 Ma to a steady background value of 176 ± 48 mW/m^2 with isolated off-axis patches of anomalous heat flow.
3. Off-axis heat flow anomalies such as Ringvent site correspond to 100–150 m deep sill intrusions elevating heat flow values locally and show evidence of hydrothermal activity.
4. While bathymetry effects are negligible, the effects of high sedimentation rates require corrections up to 20%.
5. Heat flow throughout the basin, corrected for sedimentation, shows variability in the order of ~100 mW/m^2 caused by local processes such as the presence of gas hydrate at Site U1549 and U1552 that increases heat flow and copious sedimentation that depresses heat flow.
6. Both the northern and southern transform fault of the GB do not appear to affect the thermal regime of the GB in a meaningful way.
7. Heat flow vs. plate age diagrams suggest that two primary systems control the heat transfer at the crustal scale, keeping the upper crust warm and thus facilitating rifting. An order-of-magnitude model suggests that relatively small amounts of magma are required to keep the crust weak.
8. The highly conductive rocks of the newly created crust form a deep thermal regime dominated by conduction and the cooling of gabbroic intrusions, whereas porous sediments of low thermal conductivity and permeability, form a second distinctive thermal regime that promotes the transference of heat between sills

and the ocean through hydrothermal circulation and conduction.
9. Multiple timescales control the dissipation of heat in the primary systems. We identify four characteristic time scale that describe the heat flow observations. The time interval between intrusions (ca. 10^3 yr) and the thermal relaxation time of the sills (ca. 10^4 yr) enables heat to build up in the low thermal conductivity and permeability layer. This layer, in turn, cools off at a characteristic time of 200 kyr whereas the deep thermal system controls the release of heat at timescales $>10^6$ yr.

CONFLICT OF INTEREST STATEMENT
None of the authors has a conflict of interest to disclose.

PEER REVIEW
The peer review history for this article is available at https://publons.com/publon/10.1111/bre.12755.

DATA AVAILABILITY STATEMENT
Shipboard data: https://web.iodp.tamu.edu/LORE/. Downhole logging data: https://mlp.ldeo.columbia.edu/logdb/scientific_ocean_drilling/.

ORCID
Florian Neumann https://orcid.org/0000-0002-9666-5087
Raquel Negrete-Aranda https://orcid.org/0000-0003-3049-4374
Robert N. Harris https://orcid.org/0000-0002-4641-1425
Juan Contreras https://orcid.org/0000-0002-0409-4337
Christophe Y. Galerne https://orcid.org/0000-0001-9696-205X

Manet S. Peña-Salinas 🔟 https://orcid.
org/0000-0002-5835-0455
Ronald M. Spelz 🔟 https://orcid.
org/0000-0002-9561-355X
Andreas Teske 🔟 https://orcid.org/0000-0003-3669-5425
Daniel Lizarralde 🔟 https://orcid.
org/0000-0001-6152-6039
Tobias W. Höfig 🔟 https://orcid.org/0000-0002-9254-4528

REFERENCES

Aarnes, I., Svensen, H., Connolly, J. A., & Podladchikov, Y. Y. (2010). How contact metamorphism can trigger global climate changes: Modeling gas generation around igneous sills in sedimentary basins. *Geochimica et Cosmochimica Acta*, *74*(24), 7179–7195. https://doi.org/10.1016/j.gca.2010.09.011

Aragón-Arreola, M., & Martín-Barajas, A. (2007). Westward migration of extension in the northern Gulf of California, Mexico. *Geology*, *35*(6), 571–574. https://doi.org/10.1130/G23360A.1

Beck, A. E. (1988). Methods of determining thermal conductivity and thermal diffusivity. In R. Haenel, L. Rybach, & L. Stegena (Eds.), *Handbook of terrestrial heat-flow density determination: With guidelines and recommendations of the international heat-flow commission* (pp. 87–124). Springer Netherlands. https://doi.org/10.1007/978-94-009-2847-3_4

Berndt, C., Hensen, C., Mortera-Gutierrez, C., Sarkar, S., Geilert, S., Schmidt, M., Liebetrau, V., Kipfer, R., Scholz, F., Doll, M., & Muff, S. (2016). Rifting under steam—How rift magmatism triggers methane venting from sedimentary basins. *Geology*, *44*(9), 767–770. https://doi.org/10.1130/G38049.1

Bialas, R. W., & Buck, W. R. (2009). How sediment promotes narrow rifting: Application to the Gulf of California. *Tectonics*, *28*(4), 1–18. https://doi.org/10.1029/2008TC002394

Bialas, R. W., Buck, W. R., & Qin, R. (2010). How much magma is required to rift a continent? *Earth and Planetary Science Letters*, *292*(1–2), 68–78. https://doi.org/10.1016/j.epsl.2010.01.021

Bischoff, J. L., & Henyey, T. L. (1974). Tectonic elements of the central part of the Gulf of California. *Geological Society of America Bulletin*, *85*(12), 1893–1904. https://doi.org/10.1130/0016-7606(1974)85<1893:TEOTCP>2.0.CO;2

Bredehoeft, J. D., & Papaopulos, I. S. (1965). Rates of vertical groundwater movement estimated from the Earth's thermal profile. *Water Resources Research*, *1*(2), 325–328. https://doi.org/10.1029/WR001i002p00325

Buiter, S. J., & Torsvik, T. H. (2014). A review of Wilson Cycle plate margins: A role for mantle plumes in continental break-up along sutures? *Gondwana Research*, *26*(2), 627–653. https://doi.org/10.1016/j.gr.2014.02.007

Bullard, E. C. (1939). Heat flow in South Africa. *Proceedings of the Royal Society of London*, *173*(955), 474–502. https://doi.org/10.1098/rspa.1939.0159

Calvert, S. E. (1966). Origin of diatom-rich, varved sediments from the Gulf of California. *The Journal of Geology*, *74*(5, Part 1), 546–565. https://doi.org/10.1086/627188

Čermák, V., & Rybach, L. (1982). Thermal conductivity and specific heat of minerals and rocks. In G. Angenheister (Ed.), *Landolt-Börnstein: Group V, Geophysics, Subvolume A of Volume 1, (Physical Properties of Rocks)* (pp. 305–343). Springer. https://doi.org/10.1007/10201894_62

Chen, Y. (1988). Thermal model of oceanic transform faults. *Journal of Geophysical Research: Solid Earth*, *93*(B8), 8839–8851. https://doi.org/10.1029/JB093iB08p08839

Christensen, N. I., & Salisbury, M. H. (1975). Structure and constitution of the lower oceanic crust. *Reviews of Geophysics*, *13*(1), 57–86. https://doi.org/10.1029/RG013i001p00057

Contreras-Pérez, J., Ramírez-Zerpa, N., & Negrete-Aranda, R. (2012). Modelos tectonoestratigráficos de las cuencas de Tiburón y Wagner en el norte del Golfo de California. *Revista Mexicana de Ciencias geológicas*, *29*(1), 140–157.

Courtillot, V. E., & Renne, P. R. (2003). On the ages of flood basalt events. *Comptes Rendus Geoscience*, *335*(1), 113–140. https://doi.org/10.1016/S1631-0713(03)00006-3

Crowell, J., & Gosnold, W. D. (2012, December). Using a divided bar apparatus to measure thermal conductivity of samples of odd sizes and shapes. In *AGU fall meeting abstracts* (Vol. *2012*, p. H13G-1447).

Curray, J. R., Moore, D. G., Aguayo, J. E., Aubry, M. P., Einsele, G., Fornari, D. J., Gieskes, J., Guerrero-Garcia, J., Kastner, M., Kelts, K., Lyle, M., Matoba, Y., Molina-Cruz, A., Niemitz, J., Rueda-Gaxiola, J., & Saunders, A. D. (1982a). Guaymas Basin; Sites 477, 478, and 481. In J. R. Curray, D. G. Moore, J. E. Aguayo, M.-P. Aubry, G. Einsele, D. Fornari, J. Gieskes, J. Guerrero-Garcia, M. Kastner, K. Kelts, M. Lyle, Y. Matoba, A. Molina-Cruz, J. Niemitz, J. Rueda-Gaxiola, A. Saunders, H. Schrader, B. R. T. Simoneit, & V. Vacquier (Eds.), *Initial Reports of the Deep Sea Drilling Project, 64* (pp. 211–415). Ocean Drilling Program. https://doi.org/10.2973/dsdp.proc.64.104.1982

Curray, J. R., Moore, D. G., Aguayo, J. E., Aubry, M. P., Einsele, G., Fornari, D. J., Gieskes, J., Guerrero-Garcia, J., Kastner, M., Kelts, K., Lyle, M., Matoba, Y., Molina-Cruz, A., Niemitz, J., Rueda-Gaxiola, J., & Saunders, A. D. (1982b). Guaymas Basin Slope: Sites 479 and 480. In J. R. Curray, D. G. Moore, J. E. Aguayo, M.-P. Aubry, G. Einsele, D. Fornari, J. Gieskes, J. Guerrero-Garcia, M. Kastner, K. Kelts, M. Lyle, Y. Matoba, A. Molina-Cruz, J. Niemitz, J. Rueda-Gaxiola, A. Saunders, H. Schrader, B. R. T. Simoneit, & V. Vacquier (Eds.), *Initial Reports of the Deep Sea Drilling Project, 64* (pp. 417–504). Ocean Drilling Program. https://doi.org/10.2973/dsdp.proc.64.105.1982

Davis, E. E., Villinger, H., MacDonald, R. D., Meldrum, R. D., & Grigel, J. (1997). A robust rapid-response probe for measuring bottom-hole temperatures in deep-ocean boreholes. *Marine Geophysical Researches*, *19*(3), 267–281. https://doi.org/10.1023/a:1004292930361

DeMets, C. (1995). A reappraisal of seafloor spreading lineations in the Gulf of California: Implications for the transfer of Baja California to the Pacific plate and estimates of Pacific-North America motion. *Geophysical Research Letters*, *22*(24), 3545–3548. https://doi.org/10.1029/95GL03323

Dorsey, R. J. (2010). Sedimentation and crustal recycling along an active oblique-rift margin: Salton Trough and northern Gulf of California. *Geology*, *38*(5), 443–446. https://doi.org/10.1130/G30698.1

Ebinger, C., Ayele, A., Keir, D., Rowland, J., Yirgu, G., Wright, T., Belachew, M., & Hamling, I. (2010). Length and timescales of rift faulting and magma intrusion: The Afar rifting cycle from 2005 to present. *Annual Review of Earth and Planetary Sciences*, *38*, 439–466. https://doi.org/10.1146/annurev-earth-040809-152333

Einsele, G., Gieskes, J. M., Curray, J., Moore, D. M., Aguayo, E., Aubry, M. P., Fornari, D., Guerrero, J., Kastner, M., Kelts, K., & Lyle, M. (1980). Intrusion of basaltic sills into highly porous sediments, and resulting hydrothermal activity. *Nature*, *283*(5746), 441–445. https://doi.org/10.1038/283441a0

Einsele, G., & Kelts, K. (1982). Pliocene and quaternary mud turbidites in the Gulf of California: Sedimentology, mass physical properties and significance. In J. R. Curray, D. G. Moore, J. E. Aguayo, M.-P. Aubry, G. Einsele, D. Fornari, J. Gieskes, J. Guerrero-Garcia, M. Kastner, K. Kelts, M. Lyle, Y. Matoba, A. Molina-Cruz, J. Niemitz, J. Rueda-Gaxiola, A. Saunders, H. Schrader, B. R. T. Simoneit, & V. Vacquier (Eds.), *Initial Reports of the Deep Sea Drilling Project, 64* (pp. 511–526). Ocean Drilling Program. https://doi.org/10.2973/dsdp.proc.64.107.1982

Fisher, A. T. (1998). Permeability within basaltic oceanic crust. *Reviews of Geophysics*, *36*(2), 143–182. https://doi.org/10.1029/97RG02916

Fisher, A. T., & Becker, K. (1991). Heat flow, hydrothermal circulation and basalt intrusions in the Guaymas Basin, Gulf of California. *Earth and Planetary Science Letters*, *103*(1–4), 84–99. https://doi.org/10.1016/0012-821X(91)901520-8

Forsyth, D. W., & Wilson, B. (1984). Three-dimensional temperature structure of a ridge-transform-ridge system. *Earth and Planetary Science Letters*, *70*(2), 355–362. https://doi.org/10.1016/0012-821X(84)90019-0

Fuchs, S., Balling, N., & Förster, A. (2015). Calculation of thermal conductivity, thermal diffusivity and specific heat capacity of sedimentary rocks using petrophysical well logs. *Geophysical Journal International*, *203*(3), 1977–2000. https://doi.org/10.1093/gji/ggv403

Galerne, C. Y., & Hasenclever, J. (2019). Distinct degassing pulses during magma invasion in the stratified Karoo Basin—New insights from hydrothermal fluid flow modeling. *Geochemistry, Geophysics, Geosystems*, *20*(6), 2955–2984. https://doi.org/10.1029/2018GC008120

Geilert, S., Hensen, C., Schmidt, M., Liebetrau, V., Scholz, F., Doll, M., Deng, L., Fiskal, A., Lever, M. A., Su, C. C., & Schloemer, S. (2018). On the formation of hydrothermal vents and cold seeps in the Guaymas Basin, Gulf of California. *Biogeosciences*, *15*(18), 5715–5731. https://doi.org/10.3929/ETHZ-B-000295468

Gieskes, J. M., Kastner, M., Einsele, G., Kelts, G., & Niemitz, J. (1982). Hydrothermal activity in the Guaymas Basin, Gulf of California: A synthesis. In J. R. Curray, D. G. Moore, J. E. Aguayo, M.-P. Aubry, G. Einsele, D. Fornari, J. Gieskes, J. Guerrero-Garcia, M. Kastner, K. Kelts, M. Lyle, Y. Matoba, A. Molina-Cruz, J. Niemitz, J. Rueda-Gaxiola, A. Saunders, H. Schrader, B. R. T. Simoneit, & V. Vacquier (Eds.), *Initial Reports of the Deep Sea Drilling Project, 64* (pp. 511–526). Ocean Drilling Program. https://doi.org/10.2973/dsdp.proc.64.155.1982

Goto, S., & Matsubayashi, O. (2009). Relations between the thermal properties and porosity of sediments in the eastern flank of the Juan de Fuca Ridge. *Earth, Planets and Space*, *61*(7), 863–870. https://doi.org/10.1186/BF03353197

Goutorbe, B. (2010). Combining seismically derived temperature with heat flow and bathymetry to constrain the thermal structure of oceanic lithosphere. *Earth and Planetary Science Letters*, *295*(3–4), 390–400. https://doi.org/10.1016/j.epsl.2010.04.013

Hamilton, W. (1961). Origin of the Gulf of California. *Geological Society of America Bulletin*, *72*(9), 1307–1318. https://doi.org/10.1130/0016-7606(1961)72[1307:OOTGOC]2.0.CO;2

Hasterok, D. (2013). A heat flow based cooling model for tectonic plates. *Earth and Planetary Science Letters*, *361*, 34–43. https://doi.org/10.1016/j.epsl.2012.10.036

Heesemann, M., Villinger, H., Fisher, A. T., Tréhu, A. M., & White, S. (2006). Data report: testing and deployment of the new APCT-3 tool to determine in situ temperatures while piston coring. In T. S. Collett, M. Riedel, & M. J. Malone (Eds.), *Proceedings of Integrated Ocean Drilling Program, 19* (p. 21). Integrated Ocean Drilling Program. https://doi.org/10.2204/iodp.proc.311.108.2006

Iyer, K., Rüpke, L., & Galerne, C. Y. (2013). Modeling fluid flow in sedimentary basins with sill intrusions: Implications for hydrothermal venting and climate change. *Geochemistry, Geophysics, Geosystems*, *14*(12), 5244–5262. https://doi.org/10.1002/2013GC005012

Kastner, M. (1982). Evidence for two distinct hydrothermal systems in the Guaymas Basin. In J. R. Curray, D. G. Moore, J. E. Aguayo, M.-P. Aubry, G. Einsele, D. Fornari, J. Gieskes, J. Guerrero-Garcia, M. Kastner, K. Kelts, M. Lyle, Y. Matoba, A. Molina-Cruz, J. Niemitz, J. Rueda-Gaxiola, A. Saunders, H. Schrader, B. R. T. Simoneit, & V. Vacquier (Eds.), *Initial Reports of the Deep Sea Drilling Project, 64* (pp. 1143–1158). Ocean Drilling Program. https://doi.org/10.2973/dsdp.proc.64.154.1982

Kawka, O. E., & Simoneit, B. R. T. (1987). Survey of hydrothermally-generated petroleums from the Guaymas Basin spreading center. *Organic Geochemistry*, *11*(4), 311–328. https://doi.org/10.1016/0146-6380(87)90042-8

Keenan, J. H., Keyes, F. G., Hill, P. G., & Moore, J. G. (1978). *Steam tables, SI version: Thermodynamic properties of water including vapor, liquid, and solid phases*. John Wiley & Sons Incorporated. ISBN-13: 978-0471042105.

Klitgord, K. D., Mudie, J. D., Bischoff, J. L., & Henyey, T. L. (1974). Magnetic anomalies in the northern and central Gulf of California. *Geological Society of America Bulletin*, *85*(5), 815–820. https://doi.org/10.1130/0016-7606(1974)85<815:MAITNA>2.0.CO;2

Larson, P. A., Mudie, J. D., & Larson, R. L. (1972). Magnetic anomalies and fracture-zone trends in the Gulf of California. *Geological Society of America Bulletin*, *83*(11), 3361–3368. https://doi.org/10.1130/0016-7606(1972)83[3361:MAAFTI]2.0.CO;2

Lawver, L. A., & Hawkins, J. W. (1978). Diffuse magnetic anomalies in marginal basins: Their possible tectonic and petrologic significance. *Tectonophysics*, *45*(4), 323–339. https://doi.org/10.1016/0040-1951(78)90167-1

Lawver, L. A., Sclater, J. G., Henyey, T. L., & Rogers, J. (1973). Heat flow measurements in the southern portion of the Gulf of California. *Earth and Planetary Science Letters*, *19*(2), 198–208. https://doi.org/10.1016/0012-821X(73)90115-5

Lawver, L. A., & Williams, D. L. (1979). Heat flow in the central Gulf of California. *Journal of Geophysical Research: Solid Earth*, *84*(B7), 3465–3478. https://doi.org/10.1029/JB084iB07p03465

Lawver, L. A., Williams, D. L., & Von Herzen, R. P. (1975). A major geothermal anomaly in the Gulf of California. *Nature*, *257*(5521), 23–28. https://doi.org/10.1038/257023a0

Leroy, S., Lucazeau, F., d'Acremont, E., Watremez, L., Autin, J., Rouzo, S., Bellahsen, N., Tiberi, C., Ebinger, C., Beslier, M. O., & Perrot, J. (2010). Contrasted styles of rifting in the eastern Gulf

of Aden: A combined wide-angle, multichannel seismic, and heat flow survey. *Geochemistry, Geophysics, Geosystems*, *11*(7), 1–14. https://doi.org/10.1029/2009GC002963

Levi, S., & Riddihough, R. (1986). Why are marine magnetic anomalies suppressed over sedimented spreading centers? *Geology*, *14*(8), 651–654. https://doi.org/10.1130/0091-7613(1986)14<651:WAMMAS>2.0.CO;2

Lizarralde, D., Axen, G. J., Brown, H. E., Fletcher, J. M., González-Fernández, A., Harding, A. J., Holbrook, W. S., Kent, G. M., Paramo, P., Sutherland, F., & Umhoefer, P. J. (2007). Variation in styles of rifting in the Gulf of California. *Nature*, *448*(7152), 466–469. https://doi.org/10.1038/nature06035

Lizarralde, D., Soule, S. A., Seewald, J. S., & Proskurowski, G. (2011). Carbon release by off-axis magmatism in a young sedimented spreading centre. *Nature*, *4*(1), 50–54. https://doi.org/10.1038/ngeo1006

Lonsdale, P. (1989). Geology and tectonic history of the Gulf of California. In E. L. Winterer, D. M. Hussong, & R. W. Decker (Eds.), *The Eastern Pacific Ocean and Hawaii*. Geological Society of America Boulder. https://doi.org/10.1130/DNAG-GNA-N.499

Lonsdale, P., & Becker, K. (1985). Hydrothermal plumes, hot springs, and conductive heat flow in the Southern Trough of Guaymas Basin. *Earth and Planetary Science Letters*, *73*(2–4), 211–225. https://doi.org/10.1016/0012-821X(85)90070-6

Louden, K. E., & Forsyth, D. W. (1976). Thermal conduction across fracture zones and the gravitational edge effect. *Journal of Geophysical Research*, *81*(26), 4869–4874. https://doi.org/10.1029/JB081i026p04869

MacDonald, K. C., & Atwater, T. M. (1978). Evolution of rifted ocean ridges. *Earth and Planetary Science Letters*, *39*(3), 319–327. https://doi.org/10.1016/0012-821X(78)90017-1

Morgan, J. P., & Forsyth, D. W. (1988). Three-dimensional flow and temperature perturbations due to a transform offset: Effects on oceanic crustal and upper mantle structure. *Journal of Geophysical Research: Solid Earth*, *93*(B4), 2955–2966. https://doi.org/10.1029/JB093iB04p02955

Morgan, W. J. (1983). Hotspot tracks and the early rifting of the Atlantic. *Developments in Geotectonics*, *19*, 123–139. https://doi.org/10.1016/B978-0-444-42198-2.50015-8

Negrete-Aranda, R., Contreras, J., & Spelz, R. M. (2013). Viscous dissipation, slab melting, and post-subduction volcanism in south-central Baja California, Mexico. *Geosphere*, *9*(6), 1714–1728. https://doi.org/10.1130/GES00901.1

Neumann, F., Negrete-Aranda, R., Harris, R. N., Contreras, J., Sclater, J. G., & González-Fernández, A. (2017). Systematic heat flow measurements across the Wagner Basin, northern Gulf of California. *Earth and Planetary Science Letters*, *479*, 340–353. https://doi.org/10.1016/j.epsl.2017.09.037

Parsons, B., & Sclater, J. G. (1977). An analysis of the variation of ocean floor bathymetry and heat flow with age. *Journal of Geophysical Research*, *82*(5), 803–827. https://doi.org/10.1029/JB082i005p00803

Peña-Domínguez, J. G., Negrete-Aranda, R., Neumann, F., Contreras, J., Spelz, R. M., Vega-Ramírez, L. Á., & González-Fernández, A. (2022). Heat flow and 2D multichannel seismic reflection survey of the Devil's Hole geothermal reservoir in the Wagner basin, northern Gulf of California. *Geothermics*, *103*, 102415. https://doi.org/10.1016/j.geothermics.2022.102415

Persaud, P., Di Luccio, F., & Clayton, R. W. (2015). Rayleigh wave dispersion measurements reveal low-velocity zones beneath the new crust in the Gulf of California. *Geophysical Research Letters*, *42*(6), 1766–1774. https://doi.org/10.1002/2015GL063420

Ramírez-Zerpa, N., Spelz, R. M., Yarbuh, I., Negrete-Aranda, R., Contreras, J., Clague, D. A., Neumann, F., Caress, D. W., Zierenberg, R., & González-Fernández, A. (2022). Architecture and tectonostratigraphic evolution of the Pescadero Basin Complex, southern Gulf of California: Analysis of high-resolution bathymetry data and seismic reflection profiles. *Journal of South American Earth Sciences*, *114*, 103678. https://doi.org/10.1016/j.jsames.2021.103678

Rangin, C., Desprairies, A., Fontes, J. C., Jehanno, C., & Vernhet, S. (1983). Metamorphic processes in sediments in contact with young oceanic crust—East Pacific Rise, Leg 65. In B. T. R. Lewis, P. Robinson, et al. (Eds.), *Initial Reports of the Deep Sea Drilling Project, 65* (pp. 375–389). Ocean Drilling Program. https://doi.org/10.2973/dsdp.proc.65.112.1983

Ratcliffe, E. H. (1960). The thermal conductivities of ocean sediments. *Journal of Geophysical Research*, *65*(5), 1535–1541. https://doi.org/10.1029/JZ065i005p01535

Raznjevic, K. (1976). *Handbook of thermodynamic tables and charts* (2nd ed.). Hemisphere Publishing Corporation. https://doi.org/10.1007/978-94-009-2847-3_5

Reichle, M., & Reid, I. (1977). Detailed study of earthquake swarms from the Gulf of California. *Bulletin of the Seismological Society of America*, *67*(1), 159–171. https://doi.org/10.1785/BSSA0670010159

Sass, J. H., Stone, C., & Munroe, R. J. (1984). Thermal conductivity determinations on solid rock—A comparison between a steady-state divided-bar apparatus and a commercial transient line-source device. *Journal of Volcanology and Geothermal Research*, *20*(1–2), 145–153. https://doi.org/10.1016/0377-0273(84)90071-4

Saunders, A. D., Fornari, D. J., Joron, J. L., Tarney, J., & Treuil, M. (1982). Geochemistry of basic igneous rocks, Gulf of California, Deep Sea Drilling Project Leg 64. In J. R. Curray, D. G. Moore, J. E. Aguayo, M.-P. Aubry, G. Einsele, D. Fornari, J. Gieskes, J. Guerrero-Garcia, M. Kastner, K. Kelts, M. Lyle, Y. Matoba, A. Molina-Cruz, J. Niemitz, J. Rueda-Gaxiola, A. Saunders, H. Schrader, B. R. T. Simoneit, & V. Vacquier (Eds.), *Initial Reports of the Deep Sea Drilling Project, 64* (pp. 595–642). Ocean Drilling Program. https://doi.org/10.2973/dsdp.proc.64.112.1982

Simoneit, B. R. T., & Kawka, O. E. (1987). Hydrothermal petroleum from diatomites in the Gulf of California. *Geological Society*, *26*(1), 217–228. https://doi.org/10.1144/GSL.SP.1987.026.01.14

Stein, C. A., & Stein, S. (1992). A model for the global variation in oceanic depth and heat flow with lithospheric age. *Nature*, *359*(6391), 123–129. https://doi.org/10.1038/359123a0

Stein, C. A., & Stein, S. (1994). Constraints on hydrothermal heat flux through the oceanic lithosphere from global heat flow. *Journal of Geophysical Research: Solid Earth*, *99*(B2), 3081–3095. https://doi.org/10.1029/93JB02222

Stein, J. S., & Fisher, A. T. (2001). Multiple scales of hydrothermal circulation in Middle Valley, northern Juan de Fuca Ridge: Physical constraints and geologic models. *Journal of Geophysical Research: Solid Earth*, *106*(B5), 8563–8580. https://doi.org/10.1029/2000JB900395

Stern, C., de Wit, M. J., & Lawrence, J. R. (1976). Igneous and metamorphic processes associated with the formation of Chilean ophiolites and their implication for ocean floor metamorphism, seismic layering, and magnetism. *Journal of Geophysical Research*, *81*(23), 4370–4380. https://doi.org/10.1029/JB081i023p04370

Svensen, H., Planke, S., Malthe-Sørenssen, A., Jamtveit, B., Myklebust, R., Rasmussen Eidem, T., & Rey, S. S. (2004). Release of methane from a volcanic basin as a mechanism for initial Eocene global warming. *Nature*, *429*(6991), 542–545. https://doi.org/10.1038/nature02566

Teske, A., Lizarralde, D., & Höfig, T. W. (2018). *Expedition 385 Scientific Prospectus: Guaymas Basin Tectonics and Biosphere*. International Ocean Discovery Program. https://doi.org/10.14379/iodp-sp-385-2018

Teske, A., Lizarralde, D., Höfig, T. W., Aiello, I., Ash, J., Bojanova, D., Buatier, M., Edgcomb, V. P., Galerne, C., Gontharet, S., Heuer, V. B., Jiang, S., Kars, M. A. C., Kim, J. H., Koornneef, L. M. T., Marsaglia, K., Meyer, N. R., Morono, Y., Negrete-Aranda, R., … Zhuang, G. (2021a). Expedition 385 summary. In A. Teske, D. Lizarralde, T. W. Höfig, & the Expedition 385 Scientists (Eds.), *Guaymas Basin Tectonics and Biosphere. Proceedings of the International Ocean Discovery Program*. International Ocean Discovery Program. https://doi.org/10.14379/iodp.proc.385.101.2021

Teske, A., Lizarralde, D., Höfig, T. W., Aiello, I., Ash, J., Bojanova, D., Buatier, M., Edgcomb, V. P., Galerne, C., Gontharet, S., Heuer, V. B., Jiang, S., Kars, M. A. C., Kim, J. H., Koornneef, L. M. T., Marsaglia, K., Meyer, N. R., Morono, Y., Negrete-Aranda, R., … Zhuang, G. (2021b). Expedition 385 methods. In A. Teske, D. Lizarralde, T. W. Höfig, & the Expedition 385 Scientists (Eds.), *Guaymas Basin Tectonics and Biosphere. Proceedings of the International Ocean Discovery Program*. International Ocean Discovery Program. https://doi.org/10.14379/iodp.proc.385.102.2021

Teske, A., Lizarralde, D., Höfig, T. W., Aiello, I., Ash, J., Bojanova, D., Buatier, M., Edgcomb, V. P., Galerne, C., Gontharet, S., Heuer, V. B., Jiang, S., Kars, M. A. C., Kim, J. H., Koornneef, L. M. T., Marsaglia, K., Meyer, N. R., Morono, Y., Negrete-Aranda, R., … Zhuang, G. (2021e). Sites U1547 and U1548. In A. Teske, D. Lizarralde, T. W. Höfig, & the Expedition 385 Scientists (Eds.), *Guaymas Basin Tectonics and Biosphere. Proceedings of the International Ocean Discovery Program, 385*. International Ocean Discovery Program. https://doi.org/10.14379/iodp.proc.385.105.2021

Teske, A., Lizarralde, D., Höfig, T. W., Aiello, I., Ash, J., Bojanova, D., Buatier, M., Edgcomb, V. P., Galerne, C., Gontharet, S., Heuer, V. B., Jiang, S., Kars, M. A. C., Kim, J. H., Koornneef, L. M. T., Marsaglia, K., Meyer, N. R., Morono, Y., Negrete-Aranda, R., … Zhuang, G. (2021f). Sites U1549. In A. Teske, D. Lizarralde, T. W. Höfig, & the Expedition 385 Scientists (Eds.), *Guaymas Basin Tectonics and Biosphere. Proceedings of the International Ocean Discovery Program, 385*. International Ocean Discovery Program. https://doi.org/10.14379/iodp.proc.385.106.2021

Teske, A., Lizarralde, D., Höfig, T. W., Aiello, I., Ash, J., Bojanova, D., Buatier, M., Edgcomb, V. P., Galerne, C., Gontharet, S., Heuer, V. B., Jiang, S., Kars, M. A. C., Kim, J. H., Koornneef, L. M. T., Marsaglia, K., Meyer, N. R., Morono, Y., Negrete-Aranda, R., … Zhuang, G. (2021g). Sites U1550. In A. Teske,

D. Lizarralde, T. W. Höfig, & the Expedition 385 Scientists (Eds.), *Guaymas Basin Tectonics and Biosphere. Proceedings of the International Ocean Discovery Program, 385*. International Ocean Discovery Program. https://doi.org/10.14379/iodp.proc.385.107.2021

Teske, A., Lizarralde, D., Höfig, T. W., Aiello, I., Ash, J., Bojanova, D., Buatier, M., Edgcomb, V. P., Galerne, C., Gontharet, S., Heuer, V. B., Jiang, S., Kars, M. A. C., Kim, J. H., Koornneef, L. M. T., Marsaglia, K., Meyer, N. R., Morono, Y., Negrete-Aranda, R., … Zhuang, G. (2021h). Sites U1551. In A. Teske, D. Lizarralde, T. W. Höfig, & the Expedition 385 Scientists (Eds.), *Guaymas Basin Tectonics and Biosphere. Proceedings of the International Ocean Discovery Program, 385*. International Ocean Discovery Program. https://doi.org/10.14379/iodp.proc.385.108.2021

Teske, A., Lizarralde, D., Höfig, T. W., Aiello, I., Ash, J., Bojanova, D., Buatier, M., Edgcomb, V. P., Galerne, C., Gontharet, S., Heuer, V. B., Jiang, S., Kars, M. A. C., Kim, J. H., Koornneef, L. M. T., Marsaglia, K., Meyer, N. R., Morono, Y., Negrete-Aranda, R., … Zhuang, G. (2021i). Sites U1552. In A. Teske, D. Lizarralde, T. W. Höfig, & the Expedition 385 Scientists (Eds.), *Guaymas Basin Tectonics and Biosphere. Proceedings of the International Ocean Discovery Program, 385*. International Ocean Discovery Program. https://doi.org/10.14379/iodp.proc.385.109.2021

Teske, A., McKay, L. J., Ravelo, A. C., Aiello, I., Mortera, C., Núñez-Useche, F., Canet, C., Chanton, J. P., Brunner, B., Hensen, C., & Ramírez, G. A. (2019). Characteristics and evolution of sill-driven off-axis hydrothermalism in Guaymas Basin— The Ringvent site. *Scientific Reports*, *9*(1), 1–16. https://doi.org/10.1038/s41598-019-50200-5

Umhoefer, P. J., Plattner, C., & Malservisi, R. (2020). Quantifying rates of "rifting while drifting" in the southern Gulf of California: The role of the southern Baja California microplate and its eastern boundary zone. *Lithosphere*, *12*(1), 122–132. https://doi.org/10.1130/L1132.1

Vacquier, V. (1985). The measurement of thermal conductivity of solids with a transient linear heat source on the plane surface of a poorly conducting body. *Earth and Planetary Science Letters*, *74*(2–3), 275–279. https://doi.org/10.1016/0012-821X(85)90027-5

Van Andel, T. H. (1964). Recent marine sediments of Gulf of California. In T. H. van Andel & G. G. Shor (Eds.), *Marine Geology of the Gulf of California: A Symposium (Volume 3)* (pp. 216–310). https://doi.org/10.1126/science.147.3659.725-a

Von Damm, K. L., Edmond, J. M., Grant, B., Measures, C. I., Walden, B., & Weiss, R. F. (1985). Chemistry of submarine hydrothermal solutions at 21° N, East Pacific Rise. *Geochimica et Cosmochimica Acta*, *49*(11), 2197–2220. https://doi.org/10.1016/0016-7037(85)90222-4

Von Herzen, R., & Maxwell, A. E. (1959). The measurement of thermal conductivity of deep-sea sediments by a needle-probe method. *Journal of Geophysical Research*, *64*(10), 1557–1563. https://doi.org/10.1029/JZ064i010p01557

Von Herzen, R. P. (1963). Geothermal heat flow in the Gulfs of California and Aden. *Science*, *140*(3572), 1207–1208. https://doi.org/10.1126/science.140.3572.1207

Williams, D. L., Becker, K., Lawver, L. A., & Von Herzen, R. P. (1979). Heat flow at the spreading centers of the Guaymas Basin, Gulf of California. *Journal of Geophysical Research: Solid Earth*, *84*(B12), 6757–6769. https://doi.org/10.1029/JB084iB12p06757

Wilson, M. (1997). Thermal evolution of the Central Atlantic passive margins: Continental break-up above a Mesozoic super-plume. *Journal of the Geological Society*, *154*, 491–495. https://doi.org/10.1144/gsjgs.154.3.0491

Zoth, G., & Haenel, R. (1988). Appendix: 1. In R. Haenel, L. Rybach, & L. Stegena (Eds.), *Handbook of terrestrial heat-flow density determination: With guidelines and recommendations of the international heat-flow commission* (pp. 449–468). Springer Netherlands. https://doi.org/10.1007/978-94-009-2847-3_4

SUPPORTING INFORMATION

Additional supporting information can be found online in the Supporting Information section at the end of this article.

APPENDIX

Expedition 385 Scientists: Andreas P. Teske, Daniel Lizarralde, Tobias W. Höfig, Ivano W. Aiello, Janine L. Ash, Diana P. Bojanova, Martine Buatier, Virginia P. Edgcomb, Christophe Y. Galerne, Swanne Gontharet, Verena B. Heuer, Shijun Jiang, Myriam A.C. Kars, Ji-Hoon Kim, Louise M.T. Koornneef, Kathleen M. Marsaglia, Nicolette R. Meyer, Yuki Morono, Raquel Negrete-Aranda, Florian Neumann, Lucie C. Pastor, Manet Peña-Salinas, Ligia L. Pérez Cruz, Lihua Ran, Armelle Riboulleau, John A. Sarao, Florian Schubert, S. Khogenkumar Singh, Joann M. Stock, Laurent M.A.A. Toffin, Wei Xie, Toshiro Yamanaka, Guangchao Zhuang.